Brigham Young University

BYU ScholarsArchive

2012-11-22

Deposition and Characterization of Hydrophobic Coatings

Vipul Gupta
Brigham Young University - Provo

Deposition and Characterization of Hydrophobic Coatings

Vipul Gupta

A thesis submitted to the faculty of
Brigham Young University
in partial fulfillment of the requirements for the degree of

Master of Science

Matthew R. Linford, Chair
Milton L. Lee
Robert Davis

Department of Chemistry and Biochemistry

Brigham Young University

November 2012

ABSTRACT

Deposition and Characterization of Hydrophobic Coatings

Vipul Gupta
Department of Chemistry and Biochemistry, BYU
Master of Science

Hydrophobic coatings find application in various sectors of the economy including to electronics, textiles, optical devices, and in scientific and commercial equipment. These different applications demand that different hydrophobic coatings posses a range of properties that may include smoothness or roughness, thicknesses on the order of a monolayer or a micron, robustness or the ability to dissolve quickly, transparency or opacity, water resistance or water permeability, electrical conductivity, oleophobicity, etc. However, whatever the final/desired properties, deposition via dry-deposition processes offers significant advantages, including greater reproducibility, increased environmental friendliness, and cost effectiveness on an industrial scale. Herein I explore the chemical vapor deposition of silanes and the characterization of a commercial, hydrophobic coating to better prepare and understand hydrophobic coatings on different materials.

One of the characterization techniques I used frequently in these studies is X-ray photoelectron spectroscopy (XPS). Accordingly, in Chapter 2 of this thesis I discuss this technique vis-à-vis the chemical shifts it detects, which reflect the oxidation states of materials being probed. In particular, I discuss a recommendation made over a decade ago by Gion Calzaferri for 'fixing' the problem of oxidation numbers as applied to organic materials and show how XPS confirms his suggestion.

In Chapter 3 I introduce hydrogen as an etch/cleaning gas for silicon wafers. I first show that, like argon and oxygen plasmas, hydrogen plasmas will effectively clean silicon wafers. However, I then show that hydrogen plasma treatment leads to a silicon surface that is chemically different than those prepared with the other plasmas and that undergoes silanization to a greater extent – the resulting surfaces have higher water contact angles and thicknesses.

In Chapter 4 I study the deposition of a potential barrier layer for water, which was prepared from an aza silane: N-n-butyl-aza-2,2-dimethoxysilacyclopentane (**1**) in a molecular layer deposition (MLD)-like process using either water or ammonium hydroxide as the second half reactant. This molecule has the interesting property of undergoing self-limiting growth, where the termination of this growth is accelerated by use of an ammonium hydroxide catalyst. Interestingly, films of **1** are considerably thicker on nylon than on silicon, which is explained by nylon acting as a water reservoir in the reaction.

In Chapter 5 I show the careful characterization of the hydrophobic coating on an Apple iPod nano, which was probed by ToF-SIMS, wetting, and XPS. I could identify that the coating

is only applied to the touchscreen of the device. SIMS suggested that the fluorinated coating contains oxygen, which should add to its biodegradability.

Finally, in Chapter 6 I make recommendation for future work in these areas.

Keywords: Chemical Vapor Deposition, hydrophobic coatings, water resistive barrier layer, oxidation states, silanes, XPS, glow discharge cleaning, YES 1224 P, MLD, Calzaferri approach.

ACKNOWLEDGEMENTS

First and foremost I would like to express my deep gratitude to my advisor, Dr. Matthew R. Linford. I will always be obliged to him for his undying support, brilliant guidance, and all the efforts, patience, and time he has put in me to make me gain expertise in this field of research, which was relatively new to me. I won't ever be able to forget the moments when he sat down with me and helped me through many aspects of the research not just as an advisor but more like a friend or father to me. He made every single day of my stay in his lab to be a memorable and learning experience for me. I will always be grateful to him for giving me an opportunity to work in his lab and learn under his guidance, which made these two years as one of the most memorable years of my life.

I would also like to express many thanks to my committee members: Dr. Milton L. Lee, Dr. Robert C. Davis, for all the guidance and direction they provided me throughout my journey and taking time out to review my work and help me set my goals. I would also like to thank all the faculty members of BYU, who taught and trained me on many aspects of science.

I would like to thank all the members of Dr. Linford's group for their help and support throughout my stay. I would like to mention special thanks to Dr. David S. Jensen and Dr. Gaurav Saini for training me on various instruments and technique, and for quenching my intriguing nature and welcoming my constant array of questions.

I would also like to thank the Department of Chemistry and Biochemistry for giving me an opportunity to study here and all the funding agencies and Roland K. Robins scholarship for providing all the money for my research. I would like to present my special thanks to Janet J. Fonoimoana, Susan Mortensen, and Peggy B. Erickson for helping me at various stages of my curriculum in BYU.

TABLE OF CONTENTS

List of Figures

List of Tables

Chapter 1 Introduction

1.1 Overview

My research has focused on the deposition and characterization of hydrophobic and/or barrier silane coatings on both inorganic and organic surfaces through dry deposition techniques. I have also studied the hydrophobic coating of a commercial electronic device. Hydrophobic coatings are used in various sectors of the economy, where their application is viewed as particularly important for textiles, electronics, optical devices, and various pieces of scientific, consumer, and industrial equipment. These different applications demand that different hydrophobic coatings posses a range of properties that may include smoothness or roughness, thicknesses on the order of a monolayer or a micron, robustness/abrasion resistance or the ability to dissolve quickly, transparency/invisibility or opacity, water resistance or water permeability, electrical conductivity, oleophobicity, etc. However, whatever the final properties, deposition via dry-deposition processes offers significant advantages, including greater reproducibility, increased environmental friendliness, and cost effectiveness on an industrial scale. Herein I explore the chemical vapor deposition of silanes and the characterization of a commercial, hydrophobic coating to better prepare and understand hydrophobic coatings on different materials.

Chemical vapor deposition (CVD) and atomic or molecular layer deposition (ALD or MLD) involve deposition of a desired chemical onto a surface by exposing the surface to the vapors of chemicals under vacuum conditions. Gas phase deposition is a form of dry processing, which allows its use on water sensitive devices. The vacuum lowers the boiling points of chemicals so that lower temperatures can be employed in their deposition. Vacuum conditions are often

cleaner and more reproducible than solution-based depositions. CVD, ALD, and MLD are of importance, both in research laboratories and in industry, because they are: (1) Environmentally friendly, as they minimize the amount of solvent and other chemical waste generated, (2) User friendly, as the direct interaction of the user with the chemicals is minimized, (3) Ensure surface purity, as the process takes place under vacuum, which eliminates many possible contaminants, and (4) Allow uniform, often conformal, surface coverage, as vapors at low pressure can penetrate deeply into textured/patterned/inhomogeneous/high aspect ratio materials.

Silanes can be viewed as derivatives of the molecule silane, SiH_4, from which they also derive their name. They often possess one or more hydrolytically sensitive moieties, e.g., Si-OCH_3, Si-OCH_2CH_3, or Si-Cl, which can condense with surface silanol (SiOH) groups to form siloxane (Si-O-Si) linkages. They were chosen as a preferred class of molecules for study because they offer various advantages ranging from: (1) Formation/polymerization of highly robust coatings via strong siloxane bonds, (2) Ease of control of various surface properties and/or thickness, (3) Creation of coatings that are amenable to characterization using a variety of surface analytical techniques, and (4) Are commercially available with many chain lengths and functional groups. These advantages have led to their widespread adoption, e.g., amino[1-3] and epoxy[4, 5] silanes are used in biosensors and for DNA immobilization, fluorosilanes[6, 7] and to a lesser extent alkyl silanes[8] impart hydrophobicity and oleophobicity to surfaces, some silanes are used as coupling agents,[9] and some in UV protective coatings.[10] Silanes are also used extensively as stationary phases for high performance liquid chromatography and thin layer chromatography.[11, 12]

I employed a variety of surface characterization tools in my work, including X-ray photoelectron spectroscopy (XPS), time-of-flight secondary ion mass spectrometry (ToF-SIMS), spectroscopic ellipsometric (SE), contact angle goniometry, and atomic force microscopy (AFM). The use of multiple analytical techniques helps us to piece together a more complete and informative picture of a surface/material because each technique has its particular strengths and limitations.

X-ray photoelectron spectroscopy, also known as electron spectroscopy for chemical analysis (ESCA), was invented in the mid 1960s by Kai Siegbahn, who also received a Nobel prize for his efforts. Since then it has been extensively used for the analysis of all kinds of different surfaces and materials including metals,[13, 14] polymers,[15, 16] semiconductors,[17] and ceramics.[18] XPS, as the name implies, uses X-rays to eject core electrons from the elements present at a surface/near surface region of a material. The binding energies of ejected electrons are calculated on the basis of the conservation of energy as per Equation 1, where hυ is the energy of the X-rays, B.E is the binding energy of the photoelectrons, K.E. is the kinetic energy of the electrons, which is measured by the instrument, and ϕ is the work function of the instrument, which is a small correction to the equation. The binding energies of the elements allow identification of all elements, except H and He, which the technique does not detect. It is significant that binding energies are affected by the chemical environments, i.e., oxidation states, of the atoms they come from. The use of XPS to determine the oxidation states of the elements, and in particular carbon, is explained in more detail in Chapter 2. The surface sensitivity of XPS comes from the inability of photoelectrons to travel more than ca. 10 nm in materials, which ensures the detection of electrons from only the upper most region of a surface, i.e., the technique is highly surface

sensitive. Thus, XPS is a useful method for studying surface hydrophobicity, as explained in Chapters 2 – 5.

$$h\upsilon = B.E + K.E + \phi \qquad (1)$$

ToF-SIMS, or time-of-flight secondary ion mass spectroscopy, is a form of surface mass spectrometry. Honig, Liebl and Slodzian did pioneering work in the field of ToF-SIMS[19, 20] and after fifty years of development, ToF-SIMS is widely used in different areas of science and technology including semiconductors, metals, polymers, and for biological analysis. ToF-SIMS employs a high energy beam of ions ($\sim$ 25 KeV) that bombard a surface and yield large numbers of neutral fragments as well as some secondary ions. The secondary ions produced by this ion bombardment are analyzed by a time-of-flight mass detector, which helps give the technique its name. The mass spectra generated from the secondary ions can be interpreted to provide information about the surfaces from which they come. ToF-SIMS analysis can be performed in two different modes: static and dynamic. Static SIMS is used for surface analysis of the upper ca. 2.5 nm of materials, and dynamic SIMS is used for depth profiling. Because of the large amount of information obtained in ToF-SIMS, principal components analysis (PCA) and other chemometric techniques can be used to interpret SIMS data sets from different samples (see Chapter 3).

Contact angle goniometry uses a liquid, typically water or hexadecane (HD), to probe surface hydrophobicity/hydrophillicity and/or oleophobicity/oleophilicity, respectively. A drop of the probe liquid is placed on a surface, and its sessile, advancing, or receding angle is measured by

drawing a tangent to the drop using the surface as a horizontal axis (Fig. 1.1). From this measurement, Young's equation (Eq. 2) may be used to determine the surface free energy. Young's equation is based on the principle that a body comes to rest when the vector sum of the forces acting on it are equal. The higher the contact angle, the lower the surface energy, i.e., the more hydrophobic or oleophobic the surface is. Contact angle goniometry is one of the easiest, most rapid, empirical, and inexpensive surface analytical techniques.
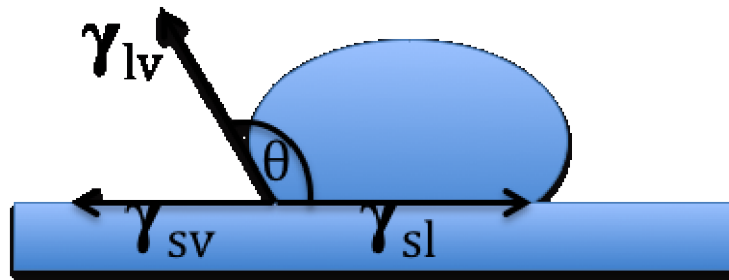
Figure 1.1 Schematic of the contact angle measurement.

$$\gamma^{sv} = \gamma^{sl} + \gamma^{lv}\cos\theta \qquad (2)$$

Spectroscopic ellipsometry (SE) is a non-contact, surface sensitive, optical technique that is used to measure film thicknesses, roughnesses, optical constants, etc. In a typical SE experiment, polarized light, of a range of wavelengths, containing both p- and s- components is directed onto a surface at an oblique angle. After reflection, the ratio of the amplitudes and the phase difference between the p- and s- components of the light are determined. These measurements give ψ and Δ, respectively. A model is then constructed of the material in question and Fresnel's laws are used to predict ψ and Δ for the model. Regression can then be used to find film thicknesses and other properties. The typical model I used in my work was an air/SiO_2/Si

construct, which used the optical constants from the instrument software for SiO_2 and Si and was adequate and appropriate for the very thin films I typically studied.

AFM or Atomic Force Microscopy is a powerful technique for surface mapping that can give topographies with a lateral resolution of <1 nm and a height resolution of < 1 Å. AFM was invented in 1986 by Binnig,[21] and since then has been widely used to study both conductive and non-conductive surfaces/materials as the technique depends on the contact forces between a tip and the sample, and not on the sample conductivity. It can even be used used on soft, biological samples[22] because of the low degree of damage caused in its tapping (tip oscillating) mode. AFM can also be operated in contact mode, which provides high-resolution images by maintaining a constant force between the surface and the tip, but this mode can scratch or damage surfaces,[23-25] and can also move particles around on surfaces to distort surface information. Tapping mode solves most of the above-mentioned problems by oscillating the tip over the surface, and hence minimizing the time of contact between the tip and the surface.[26, 27] The atomic force between the tip and surface can be calculated from the deflection of the cantilever and spring constant of the tip as per Equation 3,[28] where F is the force, S_{tip} is the spring constant of the tip, and the $Z_{deflection}$ is the deflection of the cantilever.

$$F = S_{tip} \times Z_{deflection} \tag{3}$$

1.2 Chapter 2

In Chapter 2, which has a strong tutorial flavor, I have tried to introduce some of the basic concepts of XPS and oxidation states. The understanding I gained in Chapter 2 helped with XPS data interpretation throughout the dissertation – I used XPS frequently in my work (see Chapters

3 – 5). In particular, Chapter 2 demonstrates the application of XPS (a core electron spectroscopy) in assigning oxidation states to organic molecules. Historically, the assignment of oxidation states to organic species has been problematic. However, in 1999, Calzaferri proposed a simple but elegant approach for assigning oxidation states to organic molecules on the basis of the relative electronegativities of carbon and hydrogen. Unfortunately, his proposal appears to have been largely ignored. In Chapter 2 I validate the Calzaferri approach using XPS.

1.3 Chapter 3

In this chapter, I describe a new in situ method for plasma cleaning Si/SiO_2, which is rapid, environmentally and user friendly, not corrosive to surfaces, and which also enhances the silane loading of surfaces. We opted for Si/SiO_2 substrates because they are readily available, relatively inexpensive, allow through characterization, e.g., allow ellipsometry, and resemble glass in their surface chemical properties. That is, the results from this chapter should be applicable to fields where glass substrates are employed. This chapter is before the other chapter on silane deposition because surface cleaning is generally the first step in any deposition technique and this technique was used in the subsequent work.

1.4 Chapter 4

In this chapter I describe a process for deposition of a multilayer hydrophobic coating, which not only imparts hydrophobicity to a surface, but that also imparts water resistance and limits the penetration of water to the underlying surface. Here I have explored a small organosilane as a precursor for a molecular layer deposition (MLD)-like process to form smooth, water resistive, inorganic-organic barrier layers on both inorganic and organic substrates. In particular, I show that sequential exposure of a surface to N-n-butyl-aza-2,2-dimethoxysilacyclopentane (**1**), and either water or aqueous ammonium hydroxide results in thin barrier layers that may be

7

appropriate for some micro or nano devices. Interestingly, the deposition of **1** appears to be self-limiting, which may make it useful where ultrathin films of controllable dimensions and uniformity are needed.

1.5 Chapter 5

Finally, in chapter 5 I have tried to utilize the knowledge gained in the previous chapters to analyze a hydrophobic/oleophobic coating on a commercial Apple iPod nano device. A thorough characterization of its several parts was conducted using ToF-SIMS, wetting, and XPS. This study shows that a protective, fluorinated coating is on its touchscreen, but interestingly not on other parts of the device. SIMS, in particular, suggests the use of oxygen within the fluorinated coating, which may increase its biodegradability/ environmental friendliness.

1.6 References

1.   Zhang, F.; Sautter, K.; Larsen, A. M.; Findley, D. A.; Davis, R. C.; Samha, H.; Linford, M. R., Chemical Vapor Deposition of Three Aminosilanes on Silicon Dioxide: Surface Characterization, Stability, Effects of Silane Concentration, and Cyanine Dye Adsorption. *Langmuir* **2010,** 26, (18), 14648-14654.

2.   Shircliff, R. A.; Martin, I. T.; Pankow, J. W.; Fennell, J.; Stradins, P.; Ghirardi, M. L.; Cowley, S. W.; Branz, H. M., High-Resolution X-ray Photoelectron Spectroscopy of Mixed Silane Monolayers for DNA Attachment. *ACS Applied Materials & Interfaces* **2011,** 3, (9), 3285-3292.

3.   Xie, B.; Muscat, A. J., Silylation of porous methylsilsesquioxane films in supercritical carbon dioxide. *Microelectronic Engineering* **2004,** 76, (1-4), 52-59.

4.   Dong, H.; Li, C. M.; Zhou, Q.; Sun, J. B.; Miao, J. M., Sensitive electrochemical enzyme immunoassay microdevice based on architecture of dual ring electrodes with a sensing cavity chamber. *Biosensors and Bioelectronics* **2006,** 22, (5), 621-626.

5.   Nam, Y.; Branch, D. W.; Wheeler, B. C., Epoxy-silane linking of biomolecules is simple and effective for patterning neuronal cultures. *Biosensors and Bioelectronics* **2006,** 22, (5), 589-597.

6.   Bhushan, B.; Hansford, D.; Lee, K. K. In *Surface modification of silicon and polydimethylsiloxane surfaces with vapor-phase-deposited ultrathin fluorosilane films for biomedical nanodevices*, 2006; AVS: 2006; pp 1197-1202.

7.   Saini, G.; Sautter, K.; Hild, F. E.; Pauley, J.; Linford, M. R., Two-silane chemical vapor deposition treatment of polymer (nylon) and oxide surfaces that yields hydrophobic (and

superhydrophobic), abrasion-resistant thin films. *Journal of Vacuum Science & Technology A: Vacuum, Surfaces, and Films* **2008,** 26, (5), 1224-1234.

8.   Maoz, R.; Sagiv, J., On the formation and structure of self-assembling monolayers. I. A comparative atr-wettability study of Langmuir‚ÄîBlodgett and adsorbed films on flat substrates and glass microbeads. *Journal of Colloid and Interface Science* **1984,** 100, (2), 465-496.

9.   Kaynak, C.; Celikbilek, C.; Akovali, G., Use of silane coupling agents to improve epoxy‚Äìrubber interface. *European Polymer Journal* **2003,** 39, (6), 1125-1132.

10.   Hwang, D. K.; Moon, J. H.; Shul, Y. G.; Jung, K. T.; Kim, D. H.; Lee, D. W., Scratch Resistant and Transparent UV-Protective Coating on Polycarbonate. *Journal of Sol-Gel Science and Technology* **2003,** 26, (1), 783-787.

11.   Kirkland, J. J.; Glajch, J. L.; Farlee, R. D., Synthesis and characterization of highly stable bonded phases for high-performance liquid chromatography column packings. *Analytical Chemistry* **1989,** 61, (1), 2-11.

12.   Kirkland, J. J., Development of some stationary phases for reversed-phase HPLC. *Journal of Chromatography A* **2004,** 1060, (1-2), 9-21.

13.   Fan, C. H.; Zhang, Y. C.; Zhang, Y.; Han, X.; Benny, C., [Spectroscopic characterization analysis on Cr (VI) removal mechanism by low-cost adsorbent of rice husk ash]. *Spectrosc. Spect. Anal.* **2010,** 30, (10), 2752-7.

14.   Custódio, J. V.; Agostinho, S. M. L.; Simões, A. M. P., Electrochemistry and surface analysis of the effect of benzotriazole on the cut edge corrosion of galvanized steel. *Electrochimica Acta* **2010,** 55, (20), 5523-5531.

15. Hook, A. L.; Anderson, D. G.; Langer, R.; Williams, P.; Davies, M. C.; Alexander, M. R., High throughput methods applied in biomaterial development and discovery. *Biomaterials* **2010,** 31, (2), 187-198.

16. Mishra, A. K.; Chattopadhyay, D. K.; Sreedhar, B.; Raju, K. V. S. N., FT-IR and XPS studies of polyurethane-urea-imide coatings. *Progress in Organic Coatings* **2006,** 55, (3), 231-243.

17. Hajati, S.; Tougaard, S., XPS for non-destructive depth profiling and 3D imaging of surface nanostructures. *Analytical and Bioanalytical Chemistry* **2010,** 396, (8), 2741-2755.

18. Grosvenor, A.; Cavell, R. G.; Mar, A., Bonding and Electronic Structure of Phosphides, Arsenides, and Antimonides by X-Ray Photoelectron and Absorption Spectroscopies Controlled Assembly and Modification of Inorganic Systems. In Wu, X.-T., Ed. Springer Berlin / Heidelberg: 2009; Vol. 133, pp 41-92.

19. Honig, R. E., The development of secondary ion mass spectrometry (SIMS): A retrospective. *International Journal of Mass Spectrometry and Ion Processes* **1985,** 66, (1), 31-54.

20. Liebl, H., Secondary-ion mass spectrometry and its use in depth profiling. *Journal of Vacuum Science and Technology* **1975,** 12, (1), 385-391.

21. Binnig, G.; Quate, C. F.; Gerber, C., Atomic Force Microscope. *Physical Review Letters* **1986,** 56, (9), 930-933.

22. Connell, S. D.; Smith, D. A., The atomic force microscope as a tool for studying phase separation in lipid membranes. *Mol Membr Biol* **2006,** 23, (1), 17-28.

23. García, R.; Pérez, R., Dynamic atomic force microscopy methods. *Surface Science Reports* **2002,** 47, (6–8), 197-301.

24.   Solares, S. D., Frequency and force modulation atomic force microscopy: low-impact tapping-mode imaging without bistability. *Measurment Science and Technology* **2007,** 18, (7), L9-L14.

25.   Kitamura, S. i.; Iwatsuki, M., Observation of Silicon Surfaces Using Ultrahigh-Vacuum Noncontact Atomic Force Microscopy. *Japanese Journal of Applied Physics* **1996,** 35, (Part 2, No.5B), L668-L671.

26.   Jalili, N.; Laxminarayana, K., A review of atomic force microscopy imaging systems: application to molecular metrology and biological sciences. *Mechatronics* **2004,** 14, (8), 907-945.

27.   Zhong, Q.; Inniss, D.; Kjoller, K.; Elings, V. B., Fractured polymer/silica fiber surface studied by tapping mode atomic force microscopy. *Surface Science Letters* **1993,** 290, (1–2), L688-L692.

28.   Maganov, S. N.; Whangbo, M. H., Surface analysis with STM and AFM: experimental and theoretical aspects of image analysis. *VHC, Verlagsgessellschaft* **1996**.

Chapter 2 General Agreement of Calzaferri's Recommendation for Oxidation Numbers in Organic Compounds with Core Level (C 1s) Binding Energies from X-ray Photoelectron Spectroscopy

2.1 Abstract

The traditional assignment of oxidation numbers to organic molecules is problematic. Accordingly, in 1999, Calzaferri proposed a simple and elegant solution that is based on the similar electronegativities of carbon and hydrogen: hydrogen would be assigned an oxidation number of zero when bonded to carbon. Here I show that X-ray photoelectron spectroscopy (XPS), a core electron spectroscopy that is sensitive to oxidation states of elements, confirms his suggestion. In particular, in this work I: (i) list the typical rules for assigning oxidation numbers, (ii) discuss the traditional assignment of oxidation numbers to organic molecules, (iii) review Calzaferri's solution, (iv) introduce X-ray photoelectron spectroscopy (XPS), (v) show the consistency of Calzaferri's suggestion with XPS results, (vi) provide supporting examples from the literature, (vii) provide examples from my own research, and (viii) further confirm the Calzaferri suggestion/photoelectron spectroscopy results by discussing two well-known reactions. We end by re-echoing Calzaferri's suggestion that the traditional rules for assigning oxidation numbers to organic molecules be modified.

2.2 Introduction

Oxidation numbers are widely taught in general chemistry. They comprise a useful bookkeeping tool for recognizing oxidation-reduction (redox) reactions, and for identifying the species that are oxidized or reduced in them. Oxidation numbers are often applied in inorganic chemistry. For example, hydride (H^-), hydrogen (H_2), and the hydrogen ion (H^+) have oxidation numbers of -1,

0, and +1, respectively, where these numbers correlate/can be viewed as being consistent with the very different chemistries of these three types of hydrogen. A number of articles have been published in this journal on the topic of oxidation states and oxidation numbers, including discussions of the rules for assigning oxidation numbers.[1-16]

Herein we first give a brief review of the traditional rules for assigning oxidation numbers. For inorganic species, these rules provide reasonable correlations between oxidation numbers and observed chemistry, as was noted for hydrogen above. However, when applied to organic molecules, these rules often lead to unusual, and sometimes unchemical, predictions. A few years ago, Calzaferri recognized this problem and made a simple suggestion to allow oxidation numbers to be assigned to organic species in a more sensible manner. Because of the similar electronegativities of carbon and hydrogen, hydrogen would be assigned an oxidation number of zero when bonded to carbon. In this report we show that results from X-ray photoelectron spectroscopy, a core electron spectroscopy that is sensitive to oxidation states of elements,[17, 18] support Calzaferri's recommendation. Various organic redox reactions (the addition of water to fumarate and the pinacol rearrangement) are also shown to make more sense when interpreted in this way, as compared to with the traditional rules. We repeat Calzaferri's recommendation that his approach be adopted for organic or biochemical redox reactions.

2.3 Experimental

X-ray photoelectron spectroscopy (XPS) was performed at the Pacific Northwest National Laboratory (PNNL) in the Environmental Molecular Sciences Laboratory (EMSL) using a Physical Electronics Quantera Scanning X-ray Microprobe (Chanhassen, MN). This system uses a focused, monochromatic Al Kα X-ray (1486.7 eV) source for excitation, a spherical section

analyzer, and a 32 element multichannel detection system. A 98 W X-ray beam focused to 100 μm (diameter) was rastered over a 1.3 mm x 0.1 mm rectangle on the sample. The X-ray beam is at normal incidence to the sample and the photoelectron detector is at 45° off-normal. High energy resolution spectra were collected using a pass-energy of 69.0 eV with a step size of 0.125 eV. For the Ag $3d_{5/2}$ reference line, these conditions produced a FWHM of 1.2 eV. All samples were analyzed as received.

The PET was obtained from Goodfellow Cambridge Ltd., Ermine Business Park, Huntingdon, England. The film was 0.1 mm thick and biaxially orientated.

2.4 Results and Discussion

2.4.1. Assignment of Oxidation Numbers to Inorganic Compounds

In general chemistry classes at Brigham Young University, oxidation numbers are taught with the following mnemonic: 'NAFHOP'. The rules corresponding to the letters in this mnemonic are given in order of importance; once an oxidation number has been assigned to an atom there is no need to go further.

Neutral species have oxidation numbers of zero; elemental species have oxidation numbers of zero, e.g., elemental Au, Ag, K, B, F (F_2), C, and O (O_2) have oxidation numbers of zero and we can represent metallic/elemental Au and Ag as Au(0) and Ag(0), respectively. In addition: (i) the charge of a monatomic ion is its oxidation number, e.g., the oxidation numbers of I^- and Fe^{3+} are -1 and +3, respectively, (ii) the sum of the oxidation numbers on the atoms in a polyatomic ion

must sum to the charge on the ion, and obviously (iii) the sum of the oxidation numbers on the atoms in a neutral, polyatomic molecule must sum to zero.

Alkali and alkaline earth metals have oxidation numbers of +1 and +2, respectively, in their compounds.

Fluorine has an oxidation number of -1 in its compounds. The other halogens also have oxidation numbers of -1 in their compounds, unless they are bonded to each other or to oxygen. If they are bonded to each other the more electronegative halogen gets the oxidation number of -1. Examples: (i) in $BrCl_3$, Br and Cl are assigned oxidation numbers of +3 and -1, respectively, and (ii) in $SiCl_4$, Si and Cl are assigned oxidation numbers of +4 and -1, respectively.

Hydrogen has an oxidation number +1 in all its compounds, unless it is bonded to a metal, in which case its oxidation number is -1. For example, the oxidation numbers of N and H in NH_3 are -3 and +1, respectively, and the oxidation numbers of NaH are +1 and -1, respectively.

With a few exceptions, oxygen has an oxidation number of -2 in its compounds. For example, the oxidation numbers of K, Mn, and O in $KMnO_4$ are +1, +7, and -2, respectively, and the oxidation numbers of Os and O in OsO_4 are +8 and -2, respectively. By Rules 'N.' and 'H.' above, the oxidation numbers of H and O in H_2O_2 are +1 and -1, respectively.

When main group atoms are not covered by the rules above, oxidation states are assigned using the periodic table, based on the gain or loss of electrons needed for the species to obtain noble gas configuration. Of course this is the reasoning behind most of the rules in this list.

Accordingly, the oxidation number of S in PbS should be -2, so the oxidation number of Pb must by +2 by Rule 'N.'

These rules are typical of those found in most general chemistry textbooks,[19-23] and apply quite well to most inorganic compounds. Other mnemonics used to help teach redox chemistry include: 'OIL RIG' (oxidation is loss of electrons; reduction is gain of electrons), 'LEO says GER' (loss of electrons is oxidation, gain of electrons is reduction), and 'ROLR' (Right-Oxidation-Left-Reduction)[7]

2.4.2. Assignment of Oxidation Numbers to Organic Compounds

Calzaferri[24] noted some of the unusual results that stem from assigning oxidation numbers to organic molecules using the typical rules taught in general chemistry (see above). In particular, the problems come from assigning hydrogen an oxidation number of +1 when bonded to carbon. Some of these consequences are presented in the examples below in a little more detail than Calzaferri originally gave, and the structures of the molecules discussed are given in Figure 2.1 with the carbon atoms in question in bold.

Example 1. When assigned in the traditional fashion, the oxidation numbers of the central carbon atoms in the series of alkanes: methane ($C H_4$), ethane ($CH_3 C H_3$), propane ($CH_3 C H_2 CH_3$), 2-methylpropane ($CH_3 C H(CH_3)_2$), and 2,2-dimethylpropane ($CH_3 C(CH_3)_3$) are -4, -3, -2, -1, and 0, respectively. Here we see a wider range of oxidation numbers for five chemically similar carbon atoms (all are in alkanes, sp^3 hybridized, and bonded only to C or H), compared to a narrower range of oxidation states (-1 to +1) for the three very different types of hydrogen listed above.

Example 2. When assigned in the traditional fashion, the oxidation numbers for the carbon atoms bonded to oxygen in the series of alcohols: CH_3OH, CH_3CH_2OH, $CH_3CHOH(CH_3)$, and $CH_3COH(CH_3)2$, are -2, -1, 0, and +1, respectively. A tenet of modern organic chemistry is that a given functional group behaves similarly in different organic molecules. Thus, it is hard to see how the carbon atoms bonded to oxygen in these alcohols should be so chemically different as to merit such different oxidation states.

Example 3. When assigned in the traditional fashion, the oxidation numbers of the carbon atoms bonded to oxygen in $CH_3C(O)H$ (acetaldehyde) and $CH_3C(O)CH3$ (acetone) are +1 and +2, respectively. While aldehydes and ketones do have somewhat different chemistries, they are based on the carbonyl group and so it is questionable whether these different oxidation numbers reflect a substantial difference in oxidation states. Also using the conventional rules, the carbon atoms in the carboxyl groups in formic acid ($HCOOH$) and acetic acid (CH_3COOH) show different oxidation numbers: +2 and +3, respectively. It is again hard to understand how the same functional group could show these different oxidation states. Further problems with these examples arise when one considers that methyl ($-CH_3$) groups are electron donating, so the carbon atoms in the carbonyl group of acetone and in the carboxyl group of acetic acid might be expected to have a slightly lower oxidation states than acetaldehyde and formic acid (not higher as predicted by the traditional rules), respectively.

In 1969 Jorgensen also discussed the anomaly of assigning oxidation states to homopolar bonds.[25]

2.4.3. Calzaferri's Solution

In his paper on oxidation numbers in biochemistry, Halkides noted that: "Oxidation numbers are assigned as if the more electronegative atom in a bond owned the electrons completely."[8] Calzaferri recognized the contradiction between this objective and the common practice of assigning hydrogen an oxidation state of +1 when bonded to carbon. His solution was simple, elegant, and a reflection of reality. Because of the similar Pauling electronegativities[26] of carbon (2.55) and hydrogen (2.20), he recommended that hydrogen be assigned an oxidation number of zero when bonded to carbon. Although beyond the scope of this paper, it is noteworthy that he also recommended an oxidation state of zero for hydrogen bonded to silicon (1.90), germanium (2.01), and boron (2.04).

Calzaferri's suggestion resolves the problems in the examples above. In Example 1 (Figure 2.1), if the hydrogen atoms have oxidation numbers of zero, then so do the carbon atoms, and each carbon can be represented as C(0). This result is clearly consistent with the identical hybridizations, similar reactivities, and nonpolar natures of these hydrocarbons. Indeed, we don't expect hydrogen bonding from C-H groups, but traditionally (and inconsistently) assign the same oxidation number to hydrogen whether it is bonded to N, O, or F, which do exhibit hydrogen bonding, or to carbon. In Example 2, all carbon atoms bonded to hydroxyl groups have oxidation numbers of +1: C(I), which is chemically reasonable, and all the other carbon atoms in these alcohols have oxidation numbers of zero. Note here that Calzaferri's suggestion did not change the assignment of +1 to H when it is bonded to oxygen. In Example 3, the carbonyl carbons in both compounds have oxidation numbers of +2: C(II), and the carbon atoms in both carboxylic acids have oxidation numbers of +3: C(III). Interestingly, the number of oxygen-carbon bonds on

a carbon atom in these examples (alkane: 0, alcohol: 1, carbonyl: 2, carboxyl: 3) is the oxidation state of that carbon atom, where an increase in the number of oxygen-carbon bonds at a carbon atom should increase its oxidation state. These results are also consistent with organic redox chemistry: alcohols can be oxidized to aldehydes or ketones, and aldehydes undergo oxidation to carboxylic acids. This approach further predicts that carbon atoms bonded to oxygen in ethers should be (like alcohols): C(I), and for carbon in carbonates or carbon dioxide, which have four oxygen-carbon bonds: C(IV).

2.4.4. Overview of X-ray Photoelectron Spectroscopy

X-ray photoelectron spectroscopy (XPS), also known as electron spectroscopy for chemical analysis (ESCA), utilizes the photoelectric effect and analysis of the kinetic energy distribution of the emitted photoelectrons to probe the electronic states and chemical composition of samples. The depth of the analyzed region varies with the electron mean free path, which is a function of the photoelectron energy. For a conductive sample in good electrical contact with the analyzer the kinetic energy of the ejected photoelectron (E_k) is given by the following equation:

$$E_k = h\nu - E_b - \varnothing_A \qquad (1)$$

where $h\nu$ is the energy of the incident X-rays and $\varnothing_A$ is the analyzer work function, which is generally quite small compared to E_k and E_b. Note the conservation of energy in Equation 1: the energy of the X-ray ($h\nu$) is equal to the sum of the binding and kinetic energies of the electron, with a small correction for the spectrometer.

EXAMPLE 1

METHANE (-4 / 0)   ETHANE (-3 / 0)   PROPANE (-2 / 0)   2-METHYLPROPANE (-1 / 0)   2,2-DIMETHYLPROAPNE (0 / 0)

EXAMPLE 2

METHANOL (-2 / +1)   ETHANOL (-1 / +1)   2-PROPANOL (0 / +1)   2-METHYLPROPANE-2-OL (+1 / +1)

EXAMPLE 3

ACETALDEHYDE (+1 / +2)   ACETONE (+2 / +2)   FORMIC ACID (+2 / +3)   ACETIC ACID (+3 / +3)
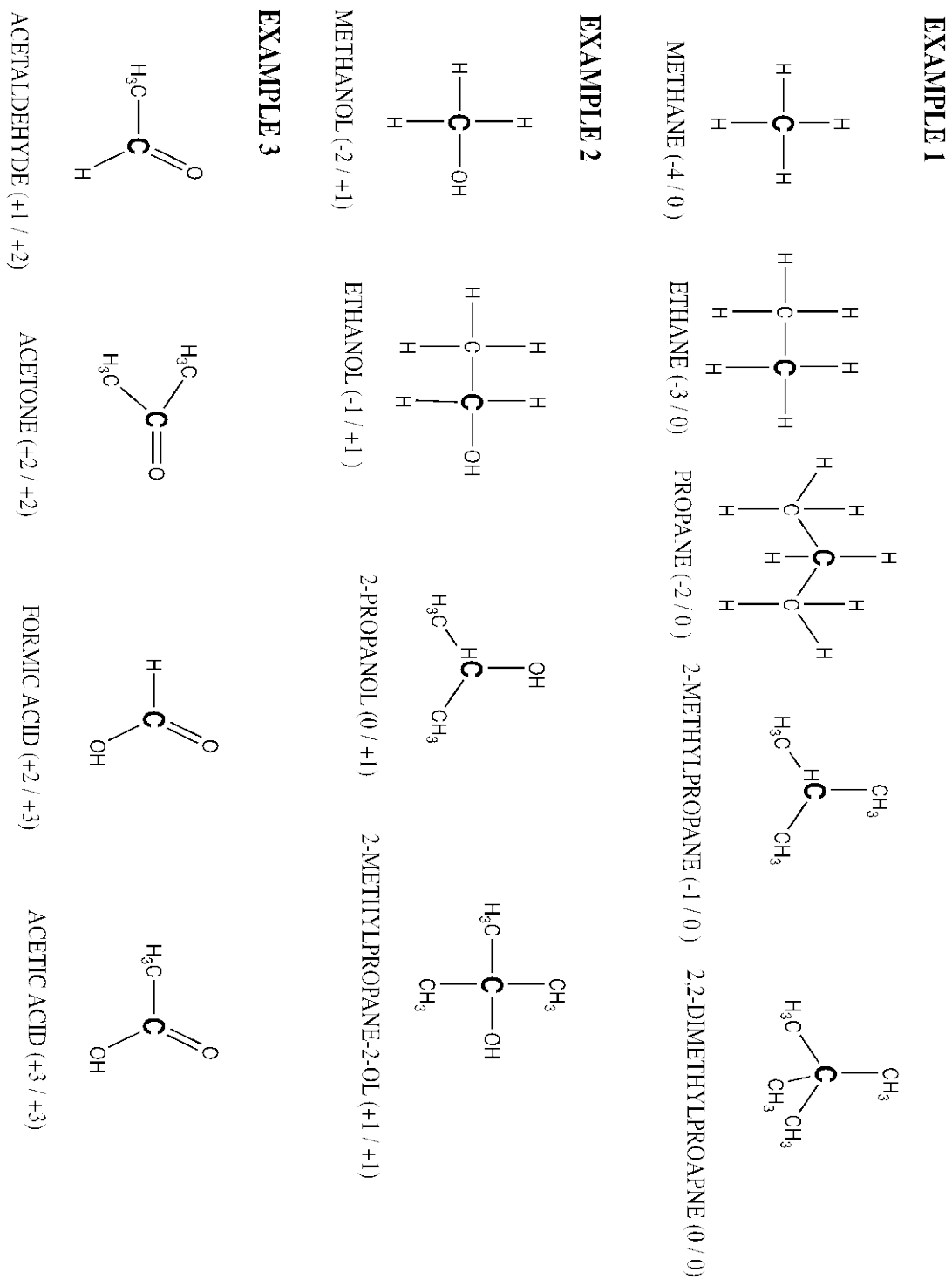
Figure 2.1 Oxidation states of different alkanes (Example 1), alcohols (Example 2), and an aldehyde, a ketone, and two carboxylic acids (Example 3). The first oxidation number in each parentheses was obtained using the traditional rules. The second number is derived from the modification proposed by Calzaferri.

21

XPS is performed under high vacuum due to the limited mean free path of the photoelectrons in air and the need to preserve many samples in a pristine state for analysis. Volatile molecules like those in Figure 2.1 are incompatible with high vacuum conditions and thus difficult to analyze using conventional XPS. Nevertheless, XPS is extremely useful for the analysis of many organic materials, including polymers,[27] monolayers,[28] and organic materials/nanomaterials,[29] e.g., carbon nanotubes.[30, 31]

The X-rays employed in most standalone XPS instruments are soft, i.e., Mg Kα = 1253.6 eV and Al Kα = 1486.6 eV. Nevertheless, these energies greatly exceed those in a typical covalent bond (ca. 4 eV), and are sufficient to eject core electrons from atoms. Using Equation 1, binding energies of atoms are calculated from E_K values measured by the electron energy analyzer. XPS is a nearly universal analysis technique – it can detect all elements except hydrogen and helium. But even though H cannot be detected, per se, its bonding often strongly affects XPS spectra.[32] No two atoms yield photoelectrons with exactly the same pattern of binding energies so atoms can be uniquely identified. XPS is also surface sensitive because the photoelectrons that are generated by the impinging X-rays cannot travel more than 2 – 3 mean free paths (MFP) in a material. Although the MFP is material and electron energy dependent, it is safe to say that at the kinetic energies expected for photoelectrons generated during XPS, the technique can only probe on the order of 10 nm (roughly three MFPs in many cases) into a material. The X-rays themselves travel much deeper. Two types of spectra are typically taken in XPS analyses: survey and narrow. Survey spectra cover a wide range of binding energies, e.g., 0 – 1100 eV, and are used to identify the various elements present in a sample. Narrow scans generally focus on a smaller, e.g., ca. 20 eV, region of a spectrum and allow information about the chemical

(oxidation) states of materials to be determined (see below). Accordingly, survey scans are typically taken at low energy resolution, while narrow scans are at high resolution. Thus, narrow scans enable the detection of changes in binding energy due to different oxidation states of the elements, known as chemical shifts. The C 1s narrow scan provides important information about the oxidation states of organic materials. The binding energy of a C 1s electron ejected from an sp^3 carbon atom bonded only to other carbon and hydrogen atoms (C-C,H) is at about 285.0 eV. Two general effects, a primary one and a secondary one, determine the binding energies of photoelectrons. The first is the shell structure of the atom and the nuclear charge, i.e., electrons will have higher binding energies if they are (i) closer to the nucleus, and (ii) attracted by a higher Z nucleus. While smaller in magnitude, the second effect, the chemical shift, is chemically more important. This effect is a result of changes in electron density around an atom that arise because of its chemical binding. For example, if atom A is bonded to a more electronegative atom, atom B, then atom A will lose some electron density to atom B. Due to this interaction, the remaining electrons in atom A will 'feel' the nuclear charge to a greater extent and be more strongly attracted to the nucleus. Accordingly, the binding energies of the electrons on atom A will increase. Depending on the number and electronegativity of the atoms bonded to an atom, the resulting chemical shifts may be 1 − 5 eV. Thus, the effects of oxidation and reduction in XPS are clear. When an atom is oxidized (or reduced), it loses (or gains) electron density, and its photoelectrons are chemically shifted to higher (or lower) binding energies. Peak fitting is commonly performed on XPS narrow scans to help identify the oxidation states of a given atom. Organic materials are usually fit with Gaussian or Gaussian-Lorentzian (Pseudo Voigt) lineshapes.[33, 34] Different oxidation states of an atom are typically assigned based on literature precedent, which is considerable, or using prior experience with a sample.

$$E_{x\text{-ray}} \approx E_{K.E} + E_{B.E}$$
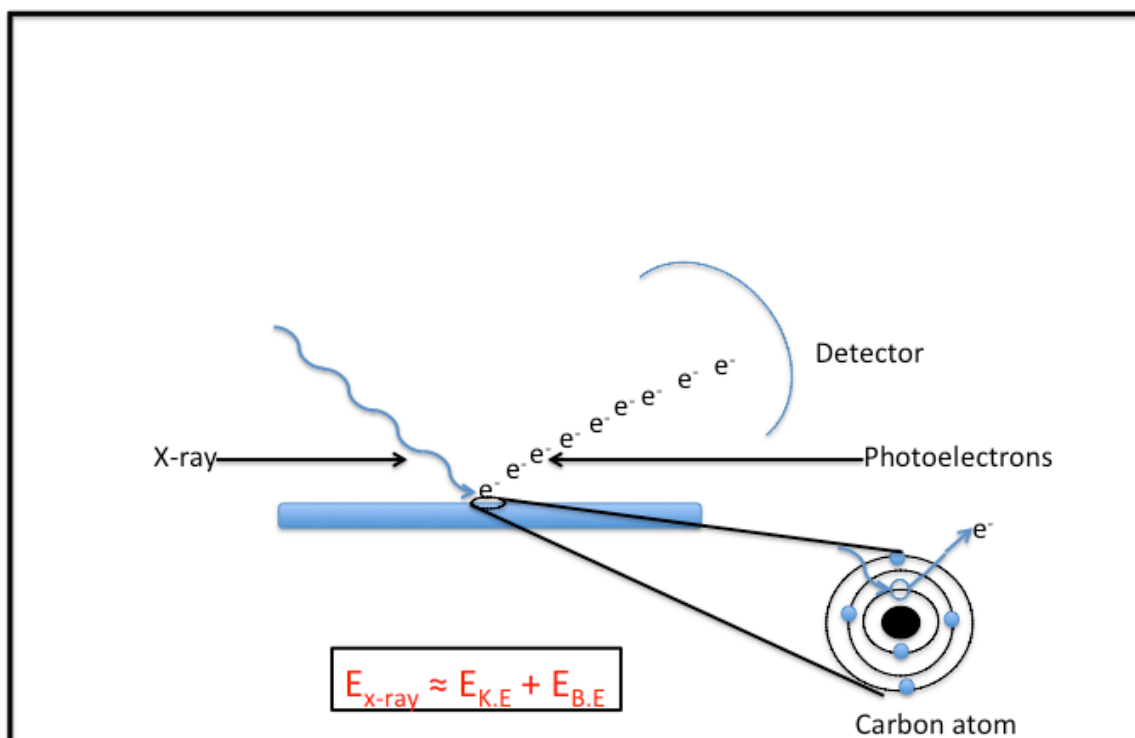
Figure 2.2 Illustration of X-ray photoelectron spectroscopy (XPS).

2.4.5. Consistency of Calzaferri's Recommendation with Results from Core Electron Spectroscopy

Because XPS has been around for decades and the functional groups in the molecules in Figure 2.1 are common, sufficient data/experience in the field exist to allow C 1s narrow scans to be reasonably predicted for the molecules in the examples in Figure 2.1.

Predicted C 1s Binding Energy Shifts of the Molecules in Example 1 (Figure 2.1) Carbon atoms bonded only to carbon or hydrogen, such as the sp^3 carbons in Example 1 show essentially the same C 1s binding energy by XPS.[35-37] In other words, all the carbon atoms in Example 1 would be experimentally found to be in essentially the same oxidation state, which is consistent with Calzaferri's recommendation and not with the conventional approach for assigning oxidation numbers to organic molecules.

Predicted C 1s Binding Energy Shifts of the Molecules in Example 2 (Figure 2.1) When carbon is bonded to oxygen, the electron density around the carbon atom decreases because of oxygen's higher electronegativity. Accordingly, it is well known, and consistent with Calzaferri's suggestion, that each oxygen bond to carbon will increase the C 1s binding energy by ca. 1.2 – 1.5 eV (for an alcohol the shift is ca. 1.5 – 1.8 eV).[38] Accordingly, one would expect one C 1s signal from methanol that would be chemically shifted ca. 1.5 eV from a C-C,H signal (the C(0) signal). The other alcohols in Example 2 would show two signals. One would be derived from carbon atoms bonded only to other carbon or hydrogen atoms and one from carbon atoms bonded to oxygen, which would be shifted to higher E_B by ca. 1.5 eV vs. C(0). The ratios of the peak areas from these signals would be representative of the number of carbon atoms in each

oxidation state. For CH₃CH₂OH, (CH₃)₂CHOH, and (CH₃)₃COH, the ratios of the signals from C-C,H and C-O would be 1:1, 2:1, and 3:1, respectively.

Predicted C 1s Binding Energy Shifts of the Molecules in Example 3 (Figure 2.1) A carbonyl (C=O) has two carbon-oxygen bonds, and a carboxyl (COOH) has three. Accordingly, the C 1s signal from a carbonyl carbon, whether from an aldehyde or a ketone, is shifted ca. 2.4 – 3.0 eV[39] from C(0), and the C 1s signal from a carboxyl carbon is shifted ca. 3.6 – 4.5 eV.[40] These observations are consistent with the +2 and +3 oxidation states predicted by Calzaferri for carbonyl and carboxyl groups, respectively.

For the carbonate group, ROC(O)OR', the chemical shift continues to increase vs. C(0) – it is ca. 5.5 – 6.7 ev.[41-43] This is consistent with the four C-O bonds to carbon in this functional group, the +4 oxidation state for this carbon predicted by Calzaferri, and the increased electron withdrawl expected from more oxygen around a carbon atom.

2.4.6. Examples from the Literature

The literature contains many examples of C 1s spectra of organic materials that confirm the analysis presented herein. A few examples follow.

XPS was performed on different polyethers, including polyethylene glycol (PEG, (CH₂CH₂O)n), polypropylene glycol (PPG, (CH₂CHCH₃O)n), and polytetramethylene glycol (PTMG, (CH₂CH₂CH₂CH₂O)n).[33] According to Calzaferri's recommendation, PEG should show carbon in a single oxidation state: +1, PPG should show carbon atoms in two oxidation states: 0 and +1 in a 1:2 ratio, respectively, and PTMG should also show carbon atoms in the C(0) and C(I)

oxidation states, but in a 1:1 ratio. All of these predictions were confirmed by XPS. For PPG, the peak positions were 285.0 eV for C(0) and 286.5 eV for C(I), showing the expected splitting of ca. 1.5 eV with the expected area ratios. The same peak splitting was observed for the two signals in the C 1s spectrum of PTMG, which had essentially equal areas. These results agree very well with Calzaferri's predictions. In contrast, the traditional approach for assigning oxidation numbers would put the three carbon atoms in the PPG repeat unit into three different oxidation states, which is chemically unreasonable and inconsistent with the experimental results.

Muir and coworkers[42] studied bisphenol A polycarbonate, peak fitting the C 1s spectrum into signals due to: aromatic (sp^2) carbon atoms bonded only to carbon or hydrogen at 284.5 eV, aliphatic (sp^3) carbon bonded only to carbon or hydrogen (C-C,H, C(0)) at 285.0 eV, the carbon atoms in the aromatic rings bonded to oxygen at 286.2 eV (consistent with the expected chemical shift of ca. 1.2 eV for C(I) vs. C(0)), and the carbonate carbon (C(IV)) at 290.4 eV, which is also chemically shifted in a reasonable way (see structure of this polymer in Figure 2.3). A discussion of the small chemical shift here between sp^2 and sp^3 carbon is beyond the scope of this paper. The ratio of these peak areas is in accordance with these different types of carbon atoms: 10:3:2:1. Calzaferri's suggestion is in reasonable agreement with these results; it places all the carbon atoms in bisphenol A polycarbonate at an oxidation state of zero, except the two connected by a single bond to oxygen (+1) and the carbonate carbon (+4). If the traditional method of assigning oxidation numbers is applied to polycarbonate, the carbon atom between the two aromatic rings is in an oxidation state of 0, those in the methyl groups attached to it are at -3,

and those in the aromatic ring (not bonded to oxygen) are at -1. It would be hard to justify these different assignments.

A few more of the many examples in the literature of C 1s spectra of organic materials include the C 1s spectra of: poly(methyl methacrylate) and poly(ether ether ketone),[44] suberoyl chloride chemisorbed onto scribed silicon,[45] oxidized carbon nanotubes,[46] and oxidized graphene.[47] All of these examples are consistent with Calzaferri's suggestion.
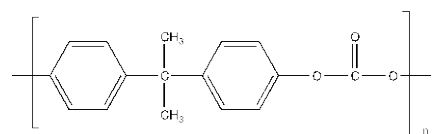
Figure 2.3 Bisphenol A polycarbonate.

2.4.7. Example of the C 1s Spectrum of Polyethylene Terephthalate

Figure 2.4 shows the structure and corresponding C 1s XPS spectrum of polyethylene terephthalate (PET) that was taken in my laboratory. The structure of PET suggests that there are carbon atoms in three different oxidation states in this polymer. One oxidation state is for carbon atoms bonded only to other carbon atoms or to hydrogen atoms. Another is in carbon bonded to one oxygen atom, and the third is from carbon bonded thrice to oxygen in the carboxyl group. Once again, Calzaferri's prediction of oxidation numbers agrees with this analysis and with the photoelectron spectroscopy. (The small secondary shift on carbons adjacent to carboxyl groups is beyond the scope of this work and not considered here.) Carbon atoms bonded only to other carbon atoms or hydrogen (those in the aromatic ring) would have oxidation states of 0 (C(0)).

Those bonded to one oxygen atom (in the ethylene unit) would have oxidation numbers of +1 (C(I)), and those in the carboxyl groups would have oxidation numbers of +3 (C(III)). The peak positions and areas in the C 1s spectrum of polyethylene terephthalate are in reasonable agreement with this analysis. The C(I) signal is chemically shifted by +1.6 eV from the C(0) signal, and the C(III) signal is chemical shifted by +2.40 eV from the C(I) signal. The ratio of the peak areas for the C(0), C(I), and C(III) signals are 0.62, 0.20, and 0.17, respectively, which is in reasonably good agreement with the 3:1:1 ratio predicted by theory. The conventional rules for assigning oxidation numbers to organic molecules would give the four inner carbon atoms of the aromatic ring (bonded only to carbon or hydrogen) and the two carbon atoms in the ethylene unit (bonded once to oxygen) the same oxidation state of -1, which is not reasonable.

2.4.8. Application to the Addition of Water to Fumarate and to the Pinacol Rearrangement

Recently in this journal, Halkides[8] and Shibley[14] discussed the conventional use of oxidation numbers in organic and bioorganic reactions.

Halkides described the addition of water to fumarate to form malate (see Figure 2.5). Based on the sum of traditionally assigned oxidation numbers on the carbon atoms of each molecule, he concluded that no net oxidation of was occurring. In contrast, the Calzaferri/photoelectron spectroscopy approach suggests that fumarate is being oxidized. One CH= group is clearly being oxidized to form a HC-OH moiety, and XPS would easily confirm the resulting chemical shift. Again, Calzaferri's approach more fully reflects reality.

Shibley[14] described the pinacol rearrangement using the traditional assignment of oxidation numbers (see Figure 2.6) as neither an oxidation nor a reduction because the oxidation level for

the molecule stays constant. Calzaferri's approach nicely shows that the carbon atoms bonded to –OH groups in the starting material are in a +1 oxidation state, and that these two carbon atoms take oxidation states of 0 and +2 in the product. While it is true that overall the oxidation state of the molecule does not change, as observed by Shibley, there most clearly is an oxidation and a reduction taking place here, which would be apparent by XPS.

2.5 Recommendation

It does not appear that Calzaferri's recommendation has been widely adopted; his paper from 1999 has only been lightly cited and we are unaware of the implementation of his recommendation in any textbooks. He suggested the following changes to the traditional rules for assigning oxidation numbers:

"For hydrogen: 0 in combination with C, Si, Ge, and also B, +1 in combination with nonmetals, -1 in combination with metals"

These changes would allow the reasonable use of oxidation numbers in organic chemistry and biochemistry. His recommendation makes sense based on atom electronegativities, and it is also consistent with photoelectron spectroscopy results. This more reasonable and logical approach should resonate with students. We echo and encourage the implementation of his suggestion.

(a)
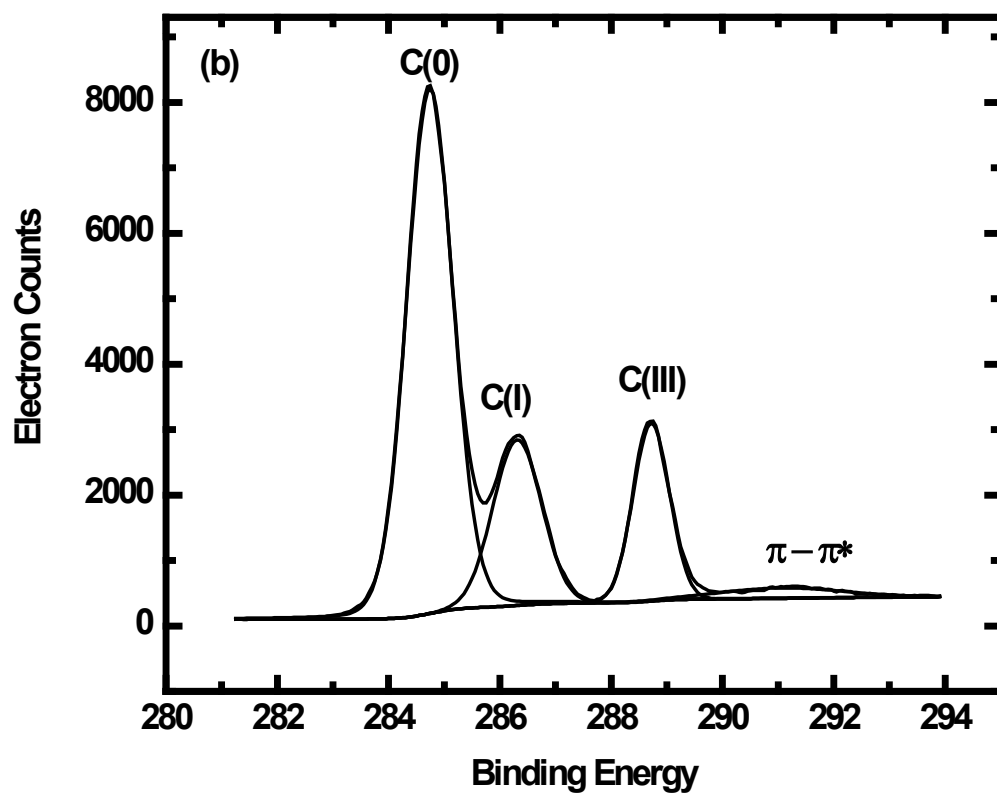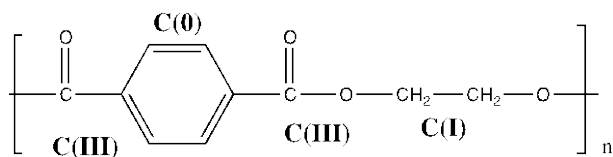
Figure 2.4 Chemical structure and C 1s XPS spectrum of polyethylene terephthalate (PET). The peak fitting shows different oxidation states for the different carbons: carbon bonded only to carbon or hydrogen (C(0)), carbon with a single bond to oxygen (C(I)), and carbon in a carboxyl group (C(III)). The π - π^* signal is commonly seen in the XPS of aromatic ring-containing materials. It is from a HOMO $\rightarrow$ LUMO transition in the ring excited by the exiting photoelectron.
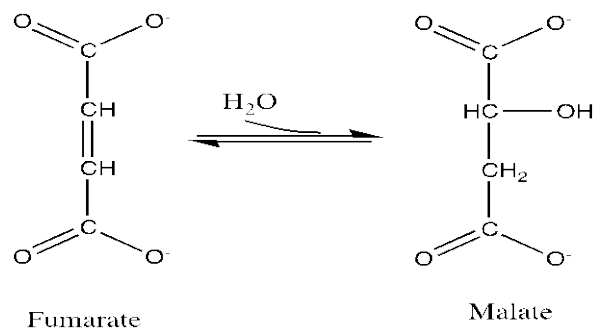
Figure 2.5 Addition of water to fumarate to make malate.

2,3-dimethylbutane-2,3-diol

3,3-dimethylbutan-2-one
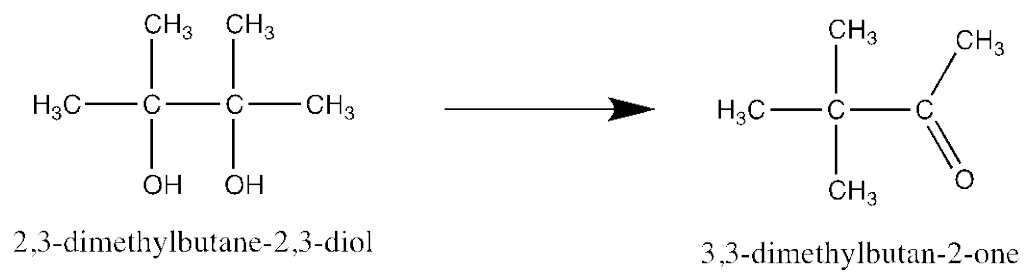
Figure 2.6 The pinacol rearrangement reaction.

2.6 Conclusions

In 2011 Loock,[13] writing in this journal, provided the following definition of oxidation states: "The oxidation state of an atom in a compound is given by the hypothetical charge of the corresponding atom or ion that is obtained by heterolytically cleaving its bond such that the atom with the higher electronegativity in a bond is allocated all electrons in the bond. Bonds between like atoms (having the same formal charge) are cleaved homolytically." Calzaferri's suggestion clearly fits this definition and provides an excellent solution to the problem of oxidation numbers in organic chemistry and biochemistry. X-ray photoelectron spectroscopy confirms the reasonableness of his proposal.

2.7 Acknowledgment

2.8 References

1.   Birk, J. P., The computer as student: An application of artificial intelligence. *Journal of Chemical Education* **1992,** 69, (4), 294.

2.   Eggert, A.; Middlecamp, C.; Kean, E., CHEMPROF: An intelligent tutor for general chemistry. *Journal of Chemical Education* **1991,** 68, (5), 403.

3.   Holleran, E. M.; Jespersen, N. D., Elementary oxidation-number rules. *Journal of Chemical Education* **1980,** 57, (9), 670.

4.   Packer, J. E.; Woodgate, S. D., Assigning oxidation numbers. *Journal of Chemical Education* **1993,** 70, (8), 691.

5.   Woolf, A. A., Oxidation numbers and their limitations. *Journal of Chemical Education* **1988,** 65, (1), 45.

6.   Kauffman, J. M., Simple method for determination of oxidation numbers of atoms in compounds. *Journal of Chemical Education* **1986,** 63, (6), 474.

7.   Stonestreet, R. H., Oxidation number for fluorine (the author responds). *Journal of Chemical Education* **1972,** 49, (4), 300.

8.   Halkides, C. J., Assigning and Using Oxidation Numbers in Biochemistry Lecture Courses. *Journal of Chemical Education* **2000,** 77, (11), 1428.

9.   Feinman, R. D., Ethanol Metabolism and the Transition from Organic Chemistry to Biochemistry. *Journal of Chemical Education* **2001,** 78, (9), 1215.

10.   Holder, D. A.; Johnson, B. G.; Karol, P. J., A Consistent Set of Oxidation Number Rules for Intelligent Computer Tutoring. *Journal of Chemical Education* **2002,** 79, (4), 465.

11.   Steinborn, D., The Concept of Oxidation States in Metal Complexes. *Journal of Chemical Education* **2004,** 81, (8), 1148.

12.   Chirik, P. J., Preface: Forum on Redox-Active Ligands. *Inorganic Chemistry* **2011,** 50, (20), 9737-9740.

13.   Loock, H.-P., Expanded Definition of the Oxidation State. *Journal of Chemical Education* **2010,** 88, (3), 282-283.

14.   Shibley, I. A.; Amaral, K. E.; Aurentz, D. J.; McCaully, R. J., Oxidation and Reduction Reactions in Organic Chemistry. *Journal of Chemical Education* **2010,** 87, (12), 1351-1354.

15.   Parkin, G., Valence, Oxidation Number, and Formal Charge: Three Related but Fundamentally Different Concepts. *Journal of Chemical Education* **2006,** 83, (5), 791.

16.   Cox, A. L.; Cox, J. R., Determining Oxidation-Reduction on a Simple Number Line. *Journal of Chemical Education* **2002,** 79, (8), 965.

17.   Kötz, R.; Neff, H.; Stucki, S., Anodic Iridium Oxide Films: XPS‐Studies of Oxidation State Changes and. *Journal of The Electrochemical Society* **1984,** 131, (1), 72-77.

18.   Wang, S.; Chia, P.-J.; Chua, L.-L.; Zhao, L.-H.; Png, R.-Q.; Sivaramakrishnan, S.; Zhou, M.; Goh, R. G. S.; Friend, R. H.; Wee, A. T. S.; Ho, P. K. H., Band-like Transport in Surface-Functionalized Highly Solution-Processable Graphene Nanosheets. *Advanced Materials* **2008,** 20, (18), 3440-3446.

19.   Stoker, H. S., *Introduction to Chemical Principles*. New Jersey, 1999.

20.   Peter Atkins, T. O., Jonathan Rourke, Mark Weller, Fraser Armstrong, *Shriver and Atkins Inorganic Chemistry*. W.H. Freeman and Company: New York, 2006.

21.   Theodore L. Brown, H. E. L. J., Bruce E. Bursten, Catherine J. Murphy, Patrick M. Woodward, *Chemistry The Central Science*. 12th ed.; Prentice Hall: IL, 2012.

22.   Brian B. liard, R. C., *University Chemistry*. Mc-Graw-Hill Higher Education.: New York, 2009.

23.   John McMurry, R. C. F., *Chemistry*. 4th ed.; Prentice Hall: New Jersey, 2004.

24.   Calzaferri, G., Oxidation Numbers. *Journal of Chemical Education* **1999,** 76, (3), 362.

25.   Jorgensen, C. K., *Oxidation Number and Oxidation States.* Springer Verlag New York Inc., 1969, 1969.

26.   Pauling, L., *The nature of the chemical bond*. 3rd ed.; Cornell University: New York, 1960.

27.   Saini, G.; Yang, L.; Lee, M. L.; Dadson, A.; Vail, M. A.; Linford, M. R., Amino-Modified Diamond as a Durable Stationary Phase for Solid-Phase Extraction. *Analytical Chemistry* **2008,** 80, (16), 6253-6259.

28.   Zhang, F.; Sautter, K.; Larsen, A. M.; Findley, D. A.; Davis, R. C.; Samha, H.; Linford, M. R., Chemical Vapor Deposition of Three Aminosilanes on Silicon Dioxide: Surface Characterization, Stability, Effects of Silane Concentration, and Cyanine Dye Adsorption. *Langmuir* **2010,** 26, (18), 14648-14654.

29.   Zhang, F.; Gates, R. J.; Smentkowski, V. S.; Natarajan, S.; Gale, B. K.; Watt, R. K.; Asplund, M. C.; Linford, M. R., Direct Adsorption and Detection of Proteins, Including Ferritin, onto Microlens Array Patterned Bioarrays. *Journal of the American Chemical Society* **2007,** 129, (30), 9252-9253.

30.   Jensen, D. S. K., S.S.; Vail, M.A.; DAdson, A.E.; Engelhard, M.H.; Linford, M.R. , XPS of a Multiwalled Carbon Nanotube Forest Grown via Chemical Vapor Deposition from Iron Catalyst Nanoparticles. *Submitted to Surface Science Spectra*.

31.   Jensen, D. S., Engelhard, M.; Zhu, Z.; Shutta; Linford, M.R. , Jensen, D.S., Engelhard, M.; Zhu, Z.; Shutta; Linford, M.R. "Multi-Instrument Characterization of the Surfaces and

Materials in Microfabricated, Carbon Nanotube-Templated Thin Layer Chromatography Plates. *Submitted to Surface and Interface Analysis*.

32.   Kerber, S. J.; Bruckner, J. J.; Wozniak, K.; Seal, S.; Hardcastle, S.; Barr, T. L. In *The nature of hydrogen in x-ray photoelectron spectroscopy: General patterns from hydroxides to hydrogen bonding*, Mineapolis, Minnesota (USA), 1996; AVS: Mineapolis, Minnesota (USA), 1996; pp 1314-1320.

33.   Hearn, M. J.; Ratner, B. D.; Briggs, D., SIMS and XPS studies of polyurethane surfaces. 1. Preliminary studies. *Macromolecules* **1988,** 21, (10), 2950-2959.

34.   Navaneetha Pandiyaraj, K.; Selvarajan, V.; Deshmukh, R. R.; Gao, C., Adhesive properties of polypropylene (PP) and polyethylene terephthalate (PET) film surfaces treated by DC glow discharge plasma. *Vacuum* **2008,** 83, (2), 332-339.

35.   Ton-That, C.; Shard, A. G.; Teare, D. O. H.; Bradley, R. H., XPS and AFM surface studies of solvent-cast PS/PMMA blends. *Polymer* **2001,** 42, (3), 1121-1129.

36.   Liston, E. M.; Martinu, L.; Wertheimer, M. R., Plasma surface modification of polymers for improved adhesion: a critical review. *Journal of Adhesion Science and Technology* **1993,** 7, (10), 1091-1127.

37.   Gerenser, L. J., XPS studies of in situ plasma-modified polymer surfaces. *Journal of Adhesion Science and Technology* **1993,** 7, (10), 1019-1040.

38.   López, G. P.; Castner, D. G.; Ratner, B. D., XPS O 1s binding energies for polymers containing hydroxyl, ether, ketone and ester groups. *Surface and Interface Analysis* **1991,** 17, (5), 267-272.

39.   Ameen, A. P.; Ward, R. J.; Short, R. D.; Beamson, G.; Briggs, D., A high-resolution X-ray photoelectron spectroscopy study of trifluoroacetic anhydride labelling of hydroxyl groups: demonstration of the Œ≤ shift due to Óó∏OC(O)CF3. *Polymer* **1993,** 34, (9), 1795-1799.

40.   Akhter, S.; Zhou, X. L.; White, J. M., XPS study of polymer/organometallic interaction: Trimethyl aluminum on polyvinyl alcohol polymer. *Applied Surface Science* **1989,** 37, (2), 201-216.

41.   Heuer, J. K.; Stubbins, J. F., An XPS characterization of $FeCO_3$ films from CO_2 corrosion. *Corrosion Science* **1999,** 41, (7), 1231-1243.

42.   Muir, B. W.; Mc Arthur, S. L.; Thissen, H.; Simon, G. P.; Griesser, H. J.; Castner, D. G., Effects of oxygen plasma treatment on the surface of bisphenol A polycarbonate: a study using SIMS, principal component analysis, ellipsometry, XPS and AFM nanoindentation. *Surface and Interface Analysis* **2006,** 38, (8), 1186-1197.

43.   Descostes, M.; Mercier, F.; Thromat, N.; Beaucaire, C.; Gautier-Soyer, M., Use of XPS in the determination of chemical environment and oxidation state of iron and sulfur samples: constitution of a data basis in binding energies for Fe and S reference compounds and applications to the evidence of surface species of an oxidized pyrite in a carbonate medium. *Applied Surface Science* **2000,** 165, (4), 288-302.

44.   Tsougeni, K.; Vourdas, N.; Tserepi, A.; Gogolides, E.; Cardinaud, C., Mechanisms of Oxygen Plasma Nanotexturing of Organic Polymer Surfaces: From Stable Super Hydrophilic to Super Hydrophobic Surfaces. *Langmuir* **2009,** 25, (19), 11748-11759.

45.   Lua, Y.-Y.; Fillmore, W. J. J.; Yang, L.; Lee, M. V.; Savage, P. B.; Asplund, M. C.; Linford, M. R., First Reaction of a Bare Silicon Surface with Acid Chlorides and a One-Step

Preparation of Acid Chloride Terminated Monolayers on Scribed Silicon. *Langmuir* **2005,** 21, (6), 2093-2097.

46.   Xing, Y.; Li, L.; Chusuei, C. C.; Hull, R. V., Sonochemical Oxidation of Multiwalled Carbon Nanotubes. *Langmuir* **2005,** 21, (9), 4185-4190.

47.   Mattevi, C.; Eda, G.; Agnoli, S.; Miller, S.; Mkhoyan, K. A.; Celik, O.; Mastrogiovanni, D.; Granozzi, G.; Garfunkel, E.; Chhowalla, M., Evolution of Electrical, Chemical, and Structural Properties of Transparent and Conducting Chemically Derived Graphene Thin Films. *Advanced Functional Materials* **2009,** 19, (16), 2577-2583.

Chapter 3 Improved Silane deposition on Hydrogen Plasma – Treated Silicon Dioxide

3.1 Abstract

We describe a method for plasma cleaning silicon surfaces that removes adventitious organic contamination and enhances silane deposition. As shown by wetting, ellipsometry, and XPS, hydrogen, oxygen, and argon plasmas effectively clean Si/SiO_2 surfaces. However, only hydrogen plasmas appear to enhance subsequent low-pressure chemical vapor deposition of silanes in a commercial tool. Chemical differences between the surfaces were confirmed via (i) deposition of two different silanes: octyldimethylmethoxysilane and butyldimethylmethoxysilane, as evidenced by spectroscopic ellipsometry and wetting, and (ii) a principle components analysis (PCA) of ToF-SIMS data taken from the different plasma-treated surfaces. AFM shows no increase in surface roughness after H_2 or O_2 plasma treatment of Si/SiO_2. The effects of surface treatment with H_2/O_2 plasmas in different gas ratios, which should allow greater control of surface chemistry, and the duration of the H_2 plasma (complete surface treatment appeared to take place quickly) are also presented. We believe that this work is significant because of the importance of silanes as surface functionalization reagents, and in particular because of the increasing importance of gas phase silane deposition.

3.2 Introduction

Silanes are widely used as surface modification agents – they are perhaps the most widely used surface functionalization agents. They can be viewed as derivatives of the molecule silane, SiH4, from which they derive their name. They often possess one or more

hydrolytically sensitive moieties, e.g., Si-OCH$_3$, Si-OCH$_2$CH$_3$, or Si-Cl, that can condense with surface silanols (SiOH groups) to form siloxane (Si-O-Si) linkages. Amino[1-3] and epoxy[4, 5] terminated silanes are used in biosensors and for DNA immobilization, fluorosilanes[6, 7] and to a lesser extent alkyl silanes[8] impart hydrophobicity and oleophobicity to surfaces, some silanes are used as coupling agents,[9] and some in UV protective coatings.[10] Silanes are used extensively as stationary phases for high performance liquid chromatography and thin layer chromatography.[11, 12] A great deal of surface chemistry has been explored on chemisorbed silane layers.[13, 14]

Many, if not most, substrates are cleaned before silane deposition, e.g., the RCA cleans are commonly used for cleaning Si/SiO$_2$, glass, and/or fused silica (amorphous silica).[15] These cleans generally consist of mixtures of water, concentrated H$_2$O$_2$, and concentrated acids, e.g., HCl, or bases, e.g., NH$_4$OH. Cleaning removes organic contamination to expose (and perhaps simultaneously create) reactive silanols. Other important cleaning solutions include piranha solution, which is a mixture of concentrated H$_2$SO$_4$ and H$_2$O$_2$, and is a variant of the RCA cleans, and dilute, aqueous HF. Note that all of these cleaning solutions are extremely dangerous and should be handled with great care.

The aqueous cleaning solutions mentioned above work well, require only relatively inexpensive reagents available in most chemistry laboratories and/or stockrooms, and can be employed in simple glass or plastic (as appropriate) vessels. Nevertheless, they are (i) incompatible with a number of interesting applications, including the coating of consumer electronic devices or other surfaces that are chemically sensitive, (ii) require special

handling – they are dangerous, and (iii) lend themselves more to batch than continuous and/or large scale processing. As a result, other surface cleaning procedures, e.g., plasmas, have been explored and implemented.[16-19] Plasma cleaning uses an activated gas, often oxygen, argon, or air, as an etching/cleaning medium. In an appropriate pressure range, application of energy to the gas results in its breakdown, yielding a plasma that usually contains a complex mixture of ions, electrons, radicals, and excited molecules. The exact effects of these species on surfaces depends on multiple factors, including the power applied to the plasma, the chemical nature of the plasma gas or gases, the pressure of the gas (it determines mean free paths), the length of time the plasma energy is applied, the chemistry of the substrate, the temperature of the chamber, and even the geometry of the chamber and location of the substrate within it. But in spite of their complexity and the obvious need to maintain specialized equipment to generate them, plasmas enjoy a number of advantages over wet cleans. They (i) are amenable to large batch processing and sometimes even continuous processes, (ii) can be more easily applied to chemically sensitive surfaces, (iii) can clean surfaces very quickly – within minutes and often even seconds, (iv) generate very little, if any, waste, (v) generally require no rinsing or drying after cleaning, and (vi) are typically much safer than the liquid cleans considered above.[20] Plasma cleaning/etching can often be used as an in situ technique that can be integrated into larger processes. Plasma systems, including those incorporated into heated chemical vapor deposition systems, are increasingly common.[1, 7, 21]

Plasma cleaning may take place by the following possible processes: (i) A sputter-off mechanism, in which excited ions, electrons, or neutral atoms have sufficient energy to

break bonds in the system, e.g., Si-C, Si-H, Si-O, C-C, or C-H bonds, leading to sputtering from the surface, (ii) an evaporative mechanism, in which plasma ions react with surface contaminants to form volatile products, e.g., CO_2, O_2, OH, etc., or (iii) A lift off mechanism, in which ions, electrons or neutral atoms achieve sufficient energy to remove underlying oxide, which sweeps away organic contamination on top of it.[22] These mechanisms are not distinct – they usually take place simultaneously with one predominating. For the gases employed in this study, Ar works predominantly by a sputter-off mechanism (the mass of H or H_2 is too low for it to work effectively in this regime), oxygen by the evaporative mechanism, and hydrogen by the lift-off mechanism.[22] Note also that plasma treatment of Si/SiO_2 surfaces with oxygen at high powers may not only clean, but cause additional growth of silicon oxide,[23] and (ii) the commonly used O_2 or air plasmas lack the ability to introduce silanol groups onto silicon oxide surfaces, and may even remove some of them, which reduces their value as a cleaning method prior to silane deposition.

Surface silanol groups are generally important for silane deposition,[24-28] becoming critical for reactions with monofunctional silanes,[29] and under anhydrous conditions. They are somewhat less important for di- and trifunctional silanes, which can polymerize and thus may be deposited on surfaces that have few or perhaps even no silanol groups.[30] In the case of polyfunctional silanes, the amount of water present at a surface and/or in solution must be carefully controlled to avoid excessive condensation/polymerization.[31] As noted, the RCA cleans, including piranha solution, may introduce silanol groups onto silicon surfaces, but traditional air or oxygen plasma cleans should not. Accordingly, an extra hydration step

may be advisable or necessary after plasma cleaning if surface silanization is to be performed. Ideally, the cleaning and hydration steps would occur simultaneously.

Herein we describe the use of a hydrogen plasma as a precursor to silane deposition under controlled conditions at 100 °C using low-pressure chemical vapor deposition (CVD)[32-34] – gas phase silanizations are increasingly viewed as the most controllable technique for depositing these reagents.[7, 35-39] This method appears to simultaneously remove adventitious organic impurities and introduce silanol groups at silicon surfaces. To the best of our knowledge it is unique – we are unaware of another study that shows the H_2 plasma treatment of a surface for silane deposition. Addition of silanols to H_2 plasma-treated Si/SiO_2 is evidenced by higher degrees of deposition for two monomethoxysilanes, compared to surfaces treated with other plasma gases (Ar, O_2, and mixtures of H_2 and O_2). Differences in the surface chemistries of Si/SiO_2 shards cleaned with different plasmas are suggested by a principal components analysis (PCA) of time-of-flight secondary ion mass spectrometry (ToF-SIMS) data.

3.3 Experimental

3.3.1 Plasma Cleaning

Silicon wafers (p-type, <100>) were from Montco Silicon Technologies, San Jose, CA. Argon,[40] oxygen,[41] hydrogen,[42] and H_2/O_2 plasmas were generated in the enclosed chamber of a YES 1224P tool (Yield Engineering Systems, Livermore, CA) using 100 W RF power and 20 sccm flow rate of the process gas at 0.30 Torr base pressure. The ratio of H_2 to O_2 was controlled using mass flow controllers. The walls of the 1224P are grounded. For our work,

three perforated plates, or shelves: active (A), ground (G), and float (F), were positioned in the chamber with a plate configuration of AG_F. The underscore signifies a space/unoccupied position, the spacings between possible positions in the chamber are 2 cm, and the A plate was at the highest available position in the chamber. Silicon samples, ca. 2.5 cm x 2.5 cm, were loaded on the center of the float plate, where the plasma does not appear to oxidize Si/SiO_2.[23]

3.3.2 CVD of Monomethoxysilanes

Two well-known silanes that can only dimerize, not polymerize, octyldimethylmethoxysilane and butyldimethylmethoxysilane (both from Gelest, Morrisville, PA), were used to test the priming/cleaning effects of the different etch gases, effectively probing the density of available silanol groups. Test shards of Si/SiO_2 for these experiments were ca. 1 in^2. The cleanliness of Si/SiO_2 shards after 60 s of plasma exposure was confirmed by measuring the thickness of the native oxide layer by spectroscopic ellipsometry and confirming that the water contact angle was below 6°. Chemical vapor deposition (CVD) was performed after in situ plasma cleaning. A CVD cycle consisted first of a 0.3 mL injection of a monomethoxysilane using the micropump assembly of the plasma/CVD instrument (YES 1224 P), where the reagent was vaporized in a vacuum flask at the side of the main chamber at 120 °C, after which the vapors were allowed to react with the Si/SiO_2 surfaces in the main chamber for 10 min at 100° C. After reaction, the silane was removed via at least 3 (often 6) pump/purge cycles (introduction of N_2 and evacuation) through a liquid N_2 cold trap. This cleaning/CVD process was repeated for Ar, O_2, and H_2 gases, and also mixtures of H_2 and O_2, after which ellipsometric thicknesses and

water contact angles were measured. To reduce the effects of cross contamination between runs, the chamber was plasma cleaned after every run for 5 min with O_2 at 100 W. To minimize the variability in the results, runs for a particular experiment were often performed in a random order on the same day. Overall, the data for this work were collected over a period of months.

3.3.3 Ellipsometry and Wetting

Film thicknesses were determined by spectroscopic ellipsometry: M-2000D, J.A. Woollam, Lincoln, NE, light sources: deuterium and quartz tungsten halogen lamps, angle of incidence of light: 75°, wavelength range: 200 nm – 1000 nm. Thicknesses were determined based on an Si/SiO_2/air model using the optical constants ($n(\lambda)$ and $k(\lambda)$) provided in the instrument software: si_jaw and sio_2_jaw, for silicon and silica, respectively. Initial and final water contact angles were measured with a contact angle goniometer: Model 100-00 Contact Angle Goniometer, Ramé-Hart, Netcong, NJ, fitted with a syringe filled with high purity water.

3.3.4 Time-of-flight secondary ion mass spectrometry (ToF-SIMS)

ToF-SIMS was performed immediately after surface treatment with an ION-TOF (Münster, Germany) TOF-SIMS IV instrument with monoisotopic 25 keV $^{69}Ga^+$ primary ions in "bunched mode." The primary ion (target) current was typically 1.8 μA, with a pulse width of 20 ns before bunching. The raster area of the beam was 100 × 100 μm^2. The peak areas of signals from H-, O-, OH-, SiO-, SiOH-, SiO^2-, SiO_2H-, SiO^3-, and SiO_3H- were measured with the instrument software (version 4.1) and normalized with respect to O- as the reference peak.

3.3.5 Principal Components Analysis (PCA) of ToF-SIMS

Data Peak areas were organized into a data matrix in Microsoft Excel. The matrix was then exported to the PLS_Toolbox 4.2 (Eigenvector Research, Inc., Wenatchee, WA) in Matlab, which autoscaled the data and performed PCA. No other preprocessing was necessary as the data were already normalized. Autoscaling is a column operation that consists of subtraction of the mean of the column of numbers from each number (mean centering), followed by division of the numbers in a column by the standard deviation of those numbers. Autoscaling seemed like an appropriate preprocessing method given our interest in understanding the effects of all the variables, independent of their magnitudes.

3.3.6 Atomic Force Microscopy

Atomic force microscopy (AFM) in tapping mode was performed on bare silicon substrates and plasma-treated silicon surfaces using a Dimension 3100 AFM (Veeco, Plainview, NY) using a tip with an Al reflective coating (OTESPA, 42 N/m, 300kHz, Bruker, Madison, WI) over a 5 μm x 5 μm area with a height scale of 10 nm.

3.3.7 X-ray Photoelectron Spectroscopy (XPS)

XPS was performed with an SSX-100 X-ray photo- electron spectrometer with a monochromatic Al K$_\alpha$ source (1486.6 eV) and a hemispherical analyzer.

3.4 Results and Discussion

3.4.1 Cleaning efficiency of different etch gases

Many surface deposition processes are sensitive to sample cleanliness; a relatively thick layer of hydrocarbon contamination will block surface silanol groups that are important in silane film growth. Plasma etch gases, such as oxygen, argon, and hydrogen are expected to remove organic contamination from surfaces.[43, 44] Figure 3.1 shows the advancing water contact angles of silicon shards before and after plasma treatment at 100 W with O_2, Ar, or H_2. These silicon surfaces had been exposed to the laboratory environment for some time and showed fairly thick contamination layers. In all cases, the water contact angles dropped to below 15° within half a minute of plasma treatment, i.e., the surfaces were wet with water. A concomitant decrease in thickness was observed by spectroscopic ellipsometry (SE), leaving the surfaces with an apparent native oxide thickness of ca. 2 nm. X-ray photoelectron spectroscopy (XPS) of the samples also showed a considerable decrease in the carbon 1s signal after surface cleaning. Surface roughnesses by AFM of the Si/SiO_2 surfaces remained essentially constant before and after plasma treatment at ca. 1.0 – 2.0 Å or lower on the hydrogen and oxygen plasma treated surfaces. While AFM after Ar plasma treatment was not performed the roughness was assumed to be similarly low.

3.4.2 Chemical vapor deposition of n-alkyldimethylmethoxysilanes

Depositions of two different monofunctional silanes on plasma treated Si/SiO_2 were studied. Monofunctional (monomethoxy) silanes were chosen because they cannot polymerize, which could complicate the results. Figure 3.2a shows a plot of the water

contact angles of Si/SiO$_2$ surfaces plasma treated with H$_2$, O$_2$, or Ar, and then exposed to gas phase octyldimethylmethoxysilane (the 'C$_8$ silane'). The C$_8$ silane has a C$_8$ chain that should yield a moderately hydrophobic surface and facilitate comparison of the different surface plasma treatments. After reaction, the surfaces treated with the hydrogen plasma have noticeably higher water contact angles (ca. 70°), suggesting greater deposition of the moderately hydrophobic C$_8$ silane, compared to those treated with either oxygen or argon (ca. 56°). The ellipsometric thicknesses of the C$_8$ silane layers deposited on the plasma-treated surfaces (Figure 3.2b) are consistent with the wetting results, showing greater thicknesses for the H$_2$ plasma/C$_8$ silane treated surfaces (ca. 2.8 Å), compared to the O$_2$ or Ar treated surfaces (increases in thickness of ca. 1.8 Å).

Deposition of a second silane, butyldimethylmethoxysilane (the 'C$_4$ silane'), was also studied using the same deposition procedure used for the C$_8$ silane. This surface reaction is also expected to increase surface hydrophobicity and leave a film of measurable thickness. Figure 3.2 shows the results of exposing H$_2$, O$_2$, and Ar plasma-treated surfaces to the C$_4$ silane. In all cases, increases in water contact angles and thicknesses, compared to unreacted samples, indicate deposition of a film. As expected, water contact angles and ellipsometric thicknesses are lower than for the reactions with the C$_8$ silane. Of greater importance, however, the H$_2$ plasma/C$_4$ silane-treated surface again shows a higher contact angle and film thickness than the surfaces treated with the other plasmas. Also as before, the O$_2$ and Ar treated surfaces showed similar contact angles and thicknesses. Results from depositions of the C$_8$ and C$_4$ silanes on Si/SiO$_2$ are consistent with the H$_2$
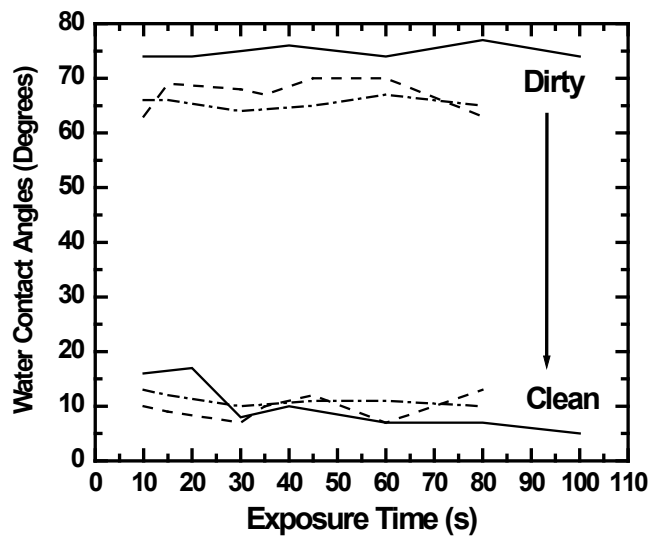
Figure 3.1 Representative water contact angle measurements of Si/SiO$_2$ surfaces before (top lines, 'dirty') and after (lower lines, 'clean') treatment with H$_2$ (solid lines), O$_2$ (dashed lines), and Ar (dash dotted lines).

(a)

(b)
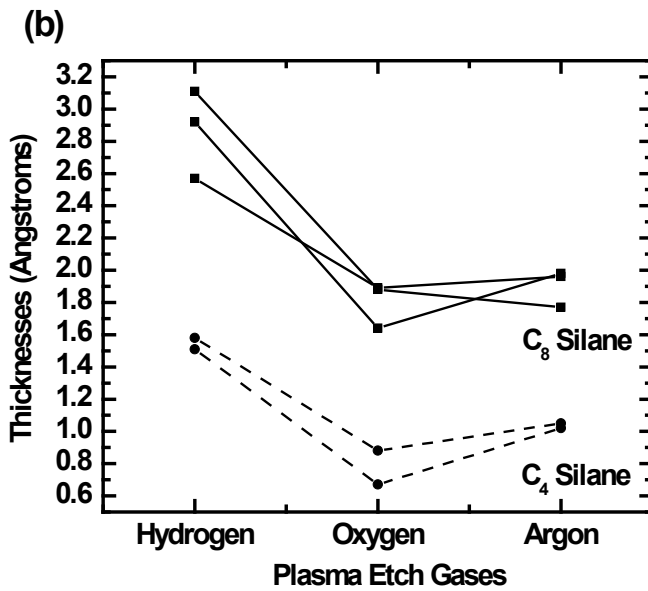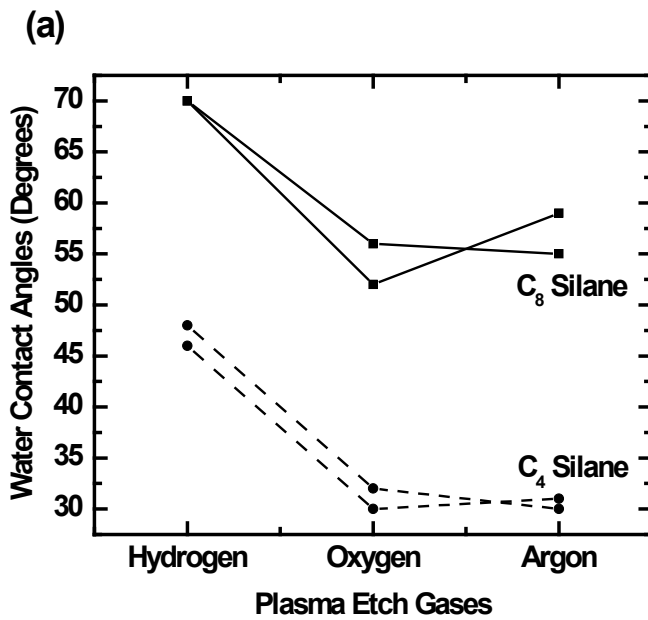
Figure 3.2 (a) Advancing water contact angles, and (b) ellipsometric thicknesses of octyldimethylmethoxysilane (C_8) (solid lines) and butyldimethylmethoxysilane (C_4) (dashed lines) silane monolayers on Si/SiO$_2$ surfaces treated with H$_2$, O$_2$, and Ar plasmas. Different lines represent different runs/sets of experiments with the 1224P instrument.

plasma introducing additional silanol groups onto silicon surfaces, the O_2 plasma removing a few of them or simply exposing them, and the Ar plasma exposing them.

3.4.3 Plasma treatment of Si/SiO$_2$ with H$_2$/O$_2$ plasmas

The results shown above leave little doubt that an H_2-treated surface more effectively primes an Si/SiO$_2$ surface for silane deposition than an O_2-treated surface. Accordingly, it was of interest to determine whether a plasma struck from a mixture of H_2 and O_2 might be even more effective for this purpose, or whether it might offer benefits not available with pure H_2 or O_2. (H_2 and O_2 are expected to react under these conditions to produce water, and this exothermic reaction is potentially dangerous. If attempting this chemistry, especially at higher pressures, one must insure that the reaction is carefully controlled and that appropriate precautions are taken.) Figure 3.3 shows water contact angles and film thicknesses for the C_4 and C_8 silanes deposited on surfaces primed with H_2/O_2 plasmas with different compositions. The general trend in these data is a decrease in water contact angles and ellipsometric thicknesses as the amount of oxygen is increased in the plasma. Thus, H_2/O_2 gas mixtures do not increase surface reactivity compared to H_2 plasmas. However, they do appear to offer the user greater control in surface priming, with a higher concentration of oxygen leading to a lower surface silane density.

3.4.4 Effects of H$_2$ plasma exposure time on silane deposition

Deposition of the C_8 silane was used to study the effect of the duration of the hydrogen plasma on silane loading. In this study, Si/SiO$_2$ surfaces were plasma treated for 30, 60, 90, and 120 s. Table 1 gives the water contact angles and thicknesses of the resulting C_8 films,

which are identical to within experimental error. That is, plasma exposure/surface saturation appears to be complete after 30 s, or if the hypothesis of this paper is correct, introduction of silanol groups is rapid and complete after this period of time. Note that these results do not agree exactly with those in Figure 3.2 because they were performed on a different silicon wafer – the results obtained herein are reproducible and consistent for a given wafer, but results from different wafers from different cassettes and/or vendors may not be directly comparable.

3.4.5 Principal Components Analysis of Time-of-Flight Secondary Ion Mass Spectrometry (ToF-SIMS) Data

While wetting and spectroscopic ellipsometry confirm surface cleaning and are rapid and convenient tools for surface analysis, they are not as chemically specific as other techniques, such as ToF-SIMS, which yields characteristic secondary ions from surfaces. Accordingly, ToF-SIMS was used to probe silicon shards directly after plasma treatment with O_2, H_2, or Ar. For better comparison of the spectra, which are often complex, a chemometrics tool, principal components analysis (PCA), was used to analyze a series of peak areas from peaks that were common to all the negative ion spectra. Chemometrics tools, including PCA, have been widely used in SIMS data analysis.[45-48] The first two principal components (PCs), i.e., PC1 and PC2, captured almost all of the variation in the data (98.55%): 78.98% and 19.57%, respectively. Obviously no higher PCs needed to be considered in this model.
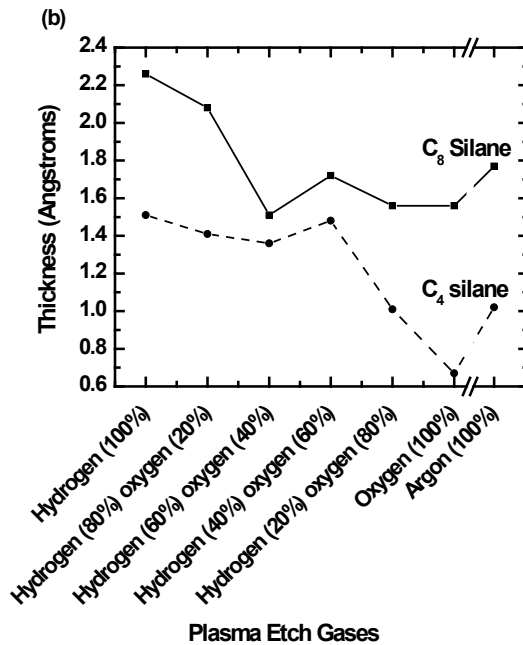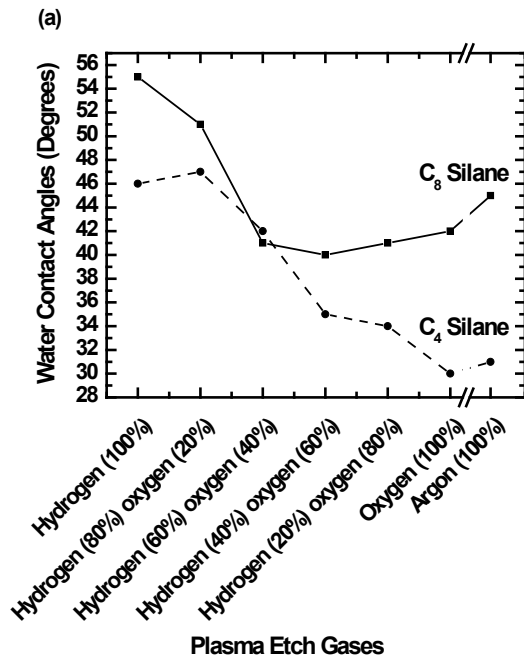
Figure 3.3 (a) Advancing water contact angles and (b) ellipsometric thicknesses of Si/SiO$_2$ surfaces treated with 100% H$_2$, 80% H$_2$/20% O$_2$, 60% H$_2$/40% O$_2$, 40% H$_2$/60% O$_2$, 20% H$_2$/80% O$_2$, 100% O$_2$, and 100% Ar (for comparison), followed by reaction with the C$_8$ (solid lines) and C$_4$ (dashed lines) silanes.

One outlying point (sample spectrum) was removed from the analysis, with the remaining points falling within 95% confidence limits in the plot of Q residuals vs. Hotelling T^2, i.e., none of the remaining points appear to be outliers. The plot of PC2 vs. PC1 (Figure 3.4) showed a clear separation between the spectra from surfaces treated with O_2, H_2, and Ar plasmas, i.e., these surfaces appear to be chemically different, which was expected from the silanization results obtained herein. In particular, the H_2 and O_2-treated samples were easily differentiated from the Ar-treated samples on PC1, but not from each other, while they were clearly different from each other on PC2. The loadings for PC1 and PC2 were also analyzed. In particular, the loadings on PC2 suggested that the H_2 plasma-treated samples showed more SiO^-, $SiOH^-$, SiO_2^-, and SiO_2H^- than the O_2 and Ar plasma-treated samples. Interestingly, the trends in Figure 3.2 correlate well with the scores on PC2 in the ToF-SIMS PCA analysis – the O_2 and Ar surfaces are similar to each other, but different from the H_2 plasma treated surface. In summary, SIMS shows chemical differences between the different plasma treated samples.

Table 3.1 Advancing water contact angles and film thicknesses for Si/SiO$_2$ surfaces treated with a hydrogen plasma for 30, 60, 90, and 120 s and then reacted with the C$_8$ silane.

Exposure Time (s)	Advancing Water Contact Angles (Degrees)	Film Thicknesses (Angstroms)
30	59	3.32
60	63	3.52
90	60	3.38
120	56	3.27

3.5 Conclusion

Plasma cleaning silicon surfaces with hydrogen, oxygen, and argon removes adventitious organic contamination, and plasma cleaning with hydrogen enhances subsequent silane deposition. Chemical differences between the surfaces were confirmed by (i) deposition of two alkyldimethylmethoxysilanes, and (ii) a PCA analysis of ToF-SIMS data taken from the different plasma-treated surfaces. AFM showed no increase in surface roughness after H_2 or O_2 plasma treatment of Si/SiO$_2$. The effects of surface treatments with H_2/O_2 plasmas in different gas ratios, which showed that increased oxygen decreased subsequent surface reactivity, and the duration of the H_2 plasma, which showed that surface priming was complete after 30 s, are presented. We believe that this work is significant because of the importance of silanes as surface functionalization reagents, and in particular because of the increasing importance of gas phase silane deposition.

3.6 Appendix 1

Surface characterization by XPS and AFM, the loadings plots on PC1 and PC2, and the plot of Q residuals vs. Hotelling T^2 can be found in the appendix 1.

3.7 Acknowledgments
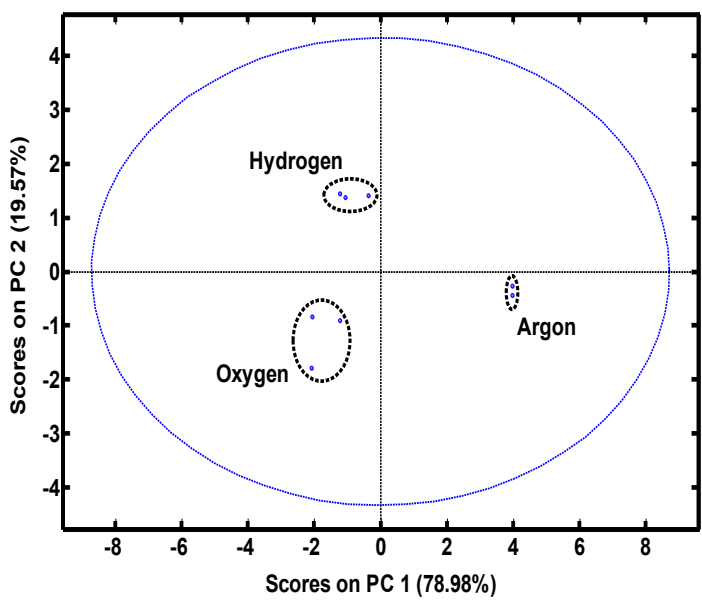
Figure 3.4 Scores on PC1 and PC2 in a PCA analysis of peak regions from negative ion ToF-SIMS spectra from substrates treated with hydrogen, oxygen, and argon plasmas, as indicated in the plot.

3.8 References

1.	Zhang, F.; Sautter, K.; Larsen, A. M.; Findley, D. A.; Davis, R. C.; Samha, H.; Linford, M. R., Chemical Vapor Deposition of Three Aminosilanes on Silicon Dioxide: Surface Characterization, Stability, Effects of Silane Concentration, and Cyanine Dye Adsorption. Langmuir 2010, 26, (18), 14648-14654.

2.	Shircliff, R. A.; Martin, I. T.; Pankow, J. W.; Fennell, J.; Stradins, P.; Ghirardi, M. L.; Cowley, S. W.; Branz, H. M., High-Resolution X-ray Photoelectron Spectroscopy of Mixed Silane Monolayers for DNA Attachment. ACS Applied Materials & Interfaces 2011, 3, (9), 3285-3292.

3.	Xie, B.; Muscat, A. J., Silylation of porous methylsilsesquioxane films in supercritical carbon dioxide. Microelectronic Engineering 2004, 76, (1-4), 52-59.

4.	Dong, H.; Li, C. M.; Zhou, Q.; Sun, J. B.; Miao, J. M., Sensitive electrochemical enzyme immunoassay microdevice based on architecture of dual ring electrodes with a sensing cavity chamber. Biosensors and Bioelectronics 2006, 22, (5), 621-626.

5.	Nam, Y.; Branch, D. W.; Wheeler, B. C., Epoxy-silane linking of biomolecules is simple and effective for patterning neuronal cultures. Biosensors and Bioelectronics 2006, 22, (5), 589-597.

6.	Bhushan, B.; Hansford, D.; Lee, K. K. In Surface modification of silicon and polydimethylsiloxane surfaces with vapor-phase-deposited ultrathin fluorosilane films for biomedical nanodevices, 2006; AVS: 2006; pp 1197-1202.

7.	Saini, G.; Sautter, K.; Hild, F. E.; Pauley, J.; Linford, M. R., Two-silane chemical vapor deposition treatment of polymer (nylon) and oxide surfaces that yields hydrophobic (and

superhydrophobic), abrasion-resistant thin films. Journal of Vacuum Science & Technology A: Vacuum, Surfaces, and Films 2008, 26, (5), 1224-1234.

8.   Maoz, R.; Sagiv, J., On the formation and structure of self-assembling monolayers. I. A comparative atr-wettability study of Langmuir,ÄîBlodgett and adsorbed films on flat substrates and glass microbeads. Journal of Colloid and Interface Science 1984, 100, (2), 465-496.

9.   Kaynak, C.; Celikbilek, C.; Akovali, G., Use of silane coupling agents to improve epoxy,Äìrubber interface. European Polymer Journal 2003, 39, (6), 1125-1132.

10.   Hwang, D. K.; Moon, J. H.; Shul, Y. G.; Jung, K. T.; Kim, D. H.; Lee, D. W., Scratch Resistant and Transparent UV-Protective Coating on Polycarbonate. Journal of Sol-Gel Science and Technology 2003, 26, (1), 783-787.

11.   Kirkland, J. J.; Glajch, J. L.; Farlee, R. D., Synthesis and characterization of highly stable bonded phases for high-performance liquid chromatography column packings. Analytical Chemistry 1989, 61, (1), 2-11.

12.   Kirkland, J. J., Development of some stationary phases for reversed-phase HPLC. Journal of Chromatography A 2004, 1060, (1-2), 9-21.

13.   Balachander, N.; Sukenik, C. N., Monolayer transformation by nucleophilic substitution: Applications to the creation of new monolayer assemblies. Langmuir 1990, 6, (11), 1621-1627.

14.   Gershevitz, O.; Sukenik, C. N.; Ghabboun, J.; Cahen, D., Molecular Monolayer-Mediated Control over Semiconductor Surfaces:,Äâ Evidence for Molecular Depolarization of Silane Monolayers on Si/SiOx. Journal of the American Chemical Society 2003, 125, (16), 4730-4731.

15.   Kern, W., The Evolution of Silicon Wafer Cleaning Technology. Journal of The Electrochemical Society 1990, 137, (6), 1887-1892.

16.   Vossen, J. L., The preparation of substrates for film deposition using glow discharge techniques. Journal of Physics E: Scientific Instruments 1979, 12, (3), 159.

17.   Aronsson, B. O.; Lausmaa, J.; Kasemo, B., Glow discharge plasma treatment for surface cleaning and modification of metallic biomaterials. Journal of Biomedical Materials Research 1997, 35, (1), 49-73.

18.   Mittal, K. L., Surface contamination: An Overview. In Surface Contamination: Genesis, Detection and Control, Mittal, K. L., Ed. Plenum Press: New York, 1979; Vol. 1, pp 3-46.

19.   L.Holland, The cleaning of glass in a glow discharge. Br. J. Appl. Phys. 1958, 9, 410-415.

20.   Petasch, W.; Kegel, B.; Schmid, H.; Lendenmann, K.; Keller, H. U., Low-pressure plasma cleaning: a process for precision cleaning applications. Surface and Coatings Technology 1997, 97, (1-3), 176-181.

21.   Quast, A. D.; Zhang, F.; Linford, M. R.; Patterson, J. E., Back-Surface Gold Mirrors for Vibrationally Resonant Sum-Frequency (VR-SFG) Spectroscopy Using 3-Mercaptopropyltrimethoxysilane as an Adhesion Promoter. Applied Spectroscopy 2011, 65, (6), 634-641.

22.   Lee, C.; Kim, H. W.; Kim, S., Organic contaminants removal by oxygen ECR plasma. Applied Surface Science 2007, 253, (7), 3658-3663.

23.   Zhang, F.; Sautter, K.; Davis, R. C.; Linford, M. R., Subsurface Oxidation for Micropatterning Silicon (SOMS). Langmuir 2009, 25, (3), 1289-1291.

24.   Sagiv, J., Organized Monolayers by Adsorption, I. Formation and Structure of Oleophobic Mixed Monolayers on Solid Surfaces. Journal of the American Chemical Society 1980, 102, (1), 92-98.

25.   Netzer, L.; Sagiv, J., A new approach to construction of artificial monolayer assemblies. Journal of the American Chemical Society 1983, 105, (3), 674-676.

26.   Angst, D. L.; Simmons, G. W., Moisture absorption characteristics of organosiloxane self-assembled monolayers. Langmuir 1991, 7, (10), 2236-2242.

27.   Allara, D. L.; Parikh, A. N.; Rondelez, F., Evidence for a Unique Chain Organization in Long Chain Silane Monolayers Deposited on Two Widely Different Solid Substrates. Langmuir 1995, 11, (7), 2357-2360.

28.   Wang, R.; Guo, J.; Baran, G.; Wunder, S. L., Characterization of the State of Order of Octadecylsilane Chains on Fumed Silica. Langmuir 1999, 16, (2), 568-576.

29.   Husseini, G. A.; Peacock, J.; Sathyapalan, A.; Zilch, L. W.; Asplund, M. C.; Sevy, E. T.; Linford, M. R., Alkyl Monolayers on Silica Surfaces Prepared Using Neat, Heated Dimethylmonochlorosilanes with Low Vapor Pressures. Langmuir 2003, 19, (12), 5169-5171.

30.   Le Grange, J. D.; Markham, J. L.; Kurkjian, C. R., Effects of surface hydration on the deposition of silane monolayers on silica. Langmuir 1993, 9, (7), 1749-1753.

31.   Silberzan, P.; Leger, L.; Ausserre, D.; Benattar, J. J., Silanation of silica surfaces. A new method of constructing pure or mixed monolayers. Langmuir 1991, 7, (8), 1647-1651.

32.   Dapkus, P. D., Metalorganic Chemical Vapor Deposition. Annual Review of Materials Science 1982, 12, (1), 243-269.

33.   Dong, J.; Wang, A.; Ng, K. Y. S.; Mao, G., Self-assembly of octadecyltrichlorosilane monolayers on silicon-based substrates by chemical vapor deposition. Thin Solid Films 2006, 515, (4), 2116-2122.

34.   Hozumi, A.; Ushiyama, K.; Sugimura, H.; Takai, O., Fluoroalkylsilane Monolayers Formed by Chemical Vapor Surface Modification on Hydroxylated Oxide Surfaces. Langmuir 1999, 15, (22), 7600-7604.

35.   Creighton, J. R.; Ho, P., Introduction to Chemical vapor Deposition (CVD). In Chemical Vapor Deposition, Park, J. H.; Sudarshan, T. S., Eds. ASM International: Materials Park, OH, 2001.

36.   Hoffmann, P. W.; Stelzle, M.; Rabolt, J. F., Vapor Phase Self-Assembly of Fluorinated Monolayers on Silicon and Germanium Oxide. Langmuir 1997, 13, (7), 1877-1880.

37.   Kanan, S. M.; Tze, W. T. Y.; Tripp, C. P., Method to Double the Surface Concentration and Control the Orientation of Adsorbed (3-Aminopropyl)dimethylethoxysilane on Silica Powders and Glass Slides. Langmuir 2002, 18, (17), 6623-6627.

38.   Pallandre, A.; Glinel, K.; Jonas, A. M.; Nysten, B., Binary Nanopatterned Surfaces Prepared from Silane Monolayers. Nano Letters 2004, 4, (2), 365-371.

39.   Ek, S.; Iiskola, E. I.; Niinisto, L.; Vaittinen, J.; Pakkanen, T. T.; Keranen, J.; Auroux, A., Atomic Layer Deposition of a High-Density Aminopropylsiloxane Network on Silica through Sequential Reactions of γ-Aminopropyltrialkoxysilanes and Water. Langmuir 2003, 19, (25), 10601-10609.

40.   Comfort, J. H.; Garverick, L. M.; Reif, R., Silicon surface cleaning by low dose argon‐ion bombardment for low‐temperature (750 °C)

epitaxial silicon deposition. I. Process considerations. Journal of Applied Physics 1987, 62, (8), 3388-3397.

41.   Oerhrlein, G. S.; Scilal, G. J.; eng, S.-J., Efficiency of oxygen plasma cleaning of reactive ion damaged silicon surfaces. Appl. Phys. Lett. 1988, 52, (11), 907-909.

42.   Park, Y.; x; Bae; Rhee, S.; Woo, Effect of hydrogen plasma precleaning on the removal of interfacial amorphous layer in the chemical vapor deposition of microcrystalline silicon films on silicon oxide surface. Applied Physics Letters 1996, 68, (16), 2219-2221.

43.   Choi, K.; Eom, T.-J.; Lee, C., Comparison of the removal efficiency for organic contaminants on silicon wafers stored in plastic boxes between UV/O3 and ECR oxygen plasma cleaning methods. Thin Solid Films 2003, 435, (1,Äì2), 227-231.

44.   M.A, B., Plasma cleaning and the removal of carbon from metal surfaces. Thin Solid Films 1980, 69, (3), 359-368.

45.   Muramoto, S.; Graham, D. J.; Wagner, M. S.; Lee, T. G.; Moon, D. W.; Castner, D. G., ToF-SIMS Analysis of Adsorbed Proteins: Principal Component Analysis of the Primary Ion Species Effect on the Protein Fragmentation Patterns. The Journal of Physical Chemistry C 2011, 115, (49), 24247-24255.

46.   Tyler, B. J.; Rayal, G.; Castner, D. G., Multivariate analysis strategies for processing ToF-SIMS images of biomaterials. Biomaterials 2007, 28, (15), 2412-2423.

47.   Yang, L.; Shirahata, N.; Saini, G.; Zhang, F.; Pei, L.; Asplund, M. C.; Kurth, D. G.; Ariga, K.; Sautter, K.; Nakanishi, T.; Smentkowski, V.; Linford, M. R., Effect of Surface Free Energy on PDMS Transfer in Microcontact Printing and Its Application to ToF-SIMS to Probe Surface Energies. Langmuir 2009, 25, (10), 5674-5683.

48.   Zhang, F.; Gates, R. J.; Smentkowski, V. S.; Natarajan, S.; Gale, B. K.; Watt, R. K.; Asplund, M. C.; Linford, M. R., Direct Adsorption and Detection of Proteins, Including Ferritin, onto Microlens Array Patterned Bioarrays. Journal of the American Chemical Society 2007, 129, (30), 9252-9253.

Chapter 4 Self-Terminating Deposition of an Aza Silane in an MLD-Like Process on Silicon and Spin-Coated Nylon

4.1 Abstract

Even a monolayer of a low surface energy species, such as a hydrocarbon or a fluorocarbon, can typically impart some measure of hydrophobicity to a surface. However, such a film is often insufficient to impart significant water resistance, which generally requires thicker films. Herein we explore a small organosilane as a precursor for a molecular layer deposition (MLD)-like process to form smooth, water resistive, inorganic-organic barrier layers on both inorganic and organic substrates. In particular, we show that sequential exposure of a surface to N-n-butyl-aza-2,2-dimethoxysilacyclopentane, and either water or aqueous ammonium hydroxide results in thin barrier layers. Interestingly, the deposition of **1** appears to be self-limiting to a few nanometers, which may make it useful where ultrathin films of controllable dimensions and uniformity are needed. Thin films were characterized using spectroscopic ellipsometry, water contact angle goniometry, X-ray photoelectron spectrosocopy, and atomic force microscopy. Film thicknesses on nylon were much higher than on silicon, and, interestingly, films prepared in the presence of 'catalyst' were thinner than those prepared with water. Test circuits coated only with a fluorosilane showed higher penetration of water compared to those coated with the barrier layer followed by the fluorosilane.

4.2 Introduction

Water resistance and repellency are important topics in the consumer electronics and textile industries, where the continued need for such coatings and barriers is driven by the convenience

and protection they provide. A very thin film, even a monolayer, of a low surface energy species, such as a hydrocarbon or a fluorocarbon, is typically enough to impart some measure of hydrophobicity to a surface. However, such ultrathin films are often insufficient to create interfaces with significant water resistance. A better solution will often involve a thicker, impermeable barrier layer.[1] Commonly employed barrier layers include paralyne,[2-7] an organic material, and various inorganic materials, i.e., different metals and metal oxides.[8-13] The paralyne coating has been reported as a barrier layer for organic thin film transistors,[14] organic light emitting diodes and solar cells,[3] and implantable medical devices[6]. It provides good water resistance, especially when it is few microns thick,[14] encapsulation,[3] biocompatibility,[6, 7] and chemical stability.[3] Nevertheless, it does not adhere well to many inorganic substrates, which makes it prone to peeling and allows lateral transport of water from edges.[3] It may also require an additional inorganic barrier for full efficacy,[4] and layers of paralyne actually absorb water and hence may hamper the purpose of water resistance.[3]

Metal oxide barrier layers have been used to prevent corrosion of metals,[8, 9] and in polymer packaging[10] and coating.[11, 12] Metal oxides can provide a good mechanical barrier for water and other species from the environment, and adhere well to most inorganic substrates.[4, 8] Nevertheless, when they are deposited by sputtering they are mostly limited to line of sight deposition,[13] and thicker coatings of metal oxides may crack, enhancing permeation of water.[8] In addition, some metal oxide coatings are not transparent,[10] which is less than preferred for consumer applications.

A possible solution to these issues might involve the use of inorganic-organic hybrid materials with inorganic moieties that might impart durability, scratch resistance, and improved adhesion to inorganic substrates, and organic moieties that could provide increased flexibility and chemical compatibility with other applications.[8] For example, Ormocer®[10, 15-18] is an inorganic-organic hybrid polymer that has been applied to ceramics, metals, and polymers.[15] It shows high abrasion resistance,[15] is a good barrier to water vapor, oxygen, flavors, etc., and has antistatic properties. A disadvantage of Ormocor®, especially for micro and nano applications, is that it is deposited by a sol-gel process.
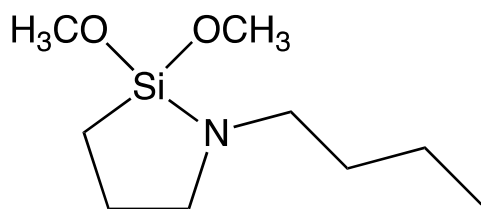
Figure 4.1 Structure of N-n-butyl-aza-2,2-dimethoxysilacyclopentane, 1.

Here I explore a small organosilane as a precursor for a molecular layer deposition[19, 20] (MLD)-like process to form smooth, water resistive, inorganic-organic barrier layers on both inorganic and organic substrates. In particular, I show that sequential exposure of a surface to N-n-butyl-aza-2,2-dimethoxysilacyclopentane, **1** (see Figure 4.1), and either water or aqueous ammonium hydroxide results in thin barrier layers that may be appropriate for some micro or nano devices. Interestingly, the deposition of **1** appears to be self-limiting to a few nanometers, which may make it useful where ultrathin films of controllable dimensions and uniformity are needed.

Each part of molecule **1** serves a useful purpose in its MLD-like deposition and/or in its final coating. For example, it would be desirable to have a moiety in molecule **1** that would be highly reactive with water, but that would not yield toxic byproducts. Highly reactive silanes often contain Si-Cl, Si-Br, or Si-N(CH$_3$)$_2$ groups, which produce toxic species when reacted with water, i.e., HCl, HBr, or NH(CH$_3$)$_2$, respectively. Part of the usefulness of molecule **1** is that it has a highly reactive Si-N linkage that will not release a toxic small molecule when exposed to water. The reaction of **1** with water is an addition reaction that opens the ring to create a species that is less volatile than **1**, which should help in film formation. The silanol group that is thus produced is then free to react with another molecule of **1** by the same ring opening reaction. The two methoxy groups on **1** are expected to slowly hydrolyze in the presence of water, and this hydrolysis, and also the subsequent condensation/polymerization that will ensue, should be catalyzed by the nitrogen atom (secondary amine) in **1**, providing some measure of robustness to the final films as they cure.[21, 22] In addition, one would expect a strong acid-base interaction between residual silanol groups and these secondary amines in the final film. Finally, the six methylene and one methyl group in the molecule provide a degree of hydrophobicity to films of **1**. However, there are not so many methylene units that the molecule does not have an appreciable vapor pressure. The ring structure of the molecule also contributes to its reasonable vapor pressure at moderate temperatures, which is essential for deposition on sensitive devices/surfaces.

Attempts were made to thoroughly characterize the MLD-like materials prepared in this study. Film growth from **1** and water or aqueous NH$_4$OH was monitored and confirmed by spectroscopic ellipsometry (SE), water contact angle goniometry, X-ray photoelectron

spectroscopy (XPS), atomic force microscopy (AFM), and time-of-flight secondary ion mass spectrometry (ToF-SIMS). The water resistivity of coatings of **1** was assayed by water immersion tests on specially designed circuits.

4.3 Experimental

4.3.1 Materials

N-n-butyl-aza-2,2-dimethoxysilacyclopentane, **1** (Gelest, Morrisville, PA), ammonium hydroxide (EMD Chemicals, Gibbstown, NJ), water (18 MΩ resistance, filtered using a Milli-Q Water System, Millipore, Billerica, MA), nylon 6 (Sigma Aldrich, St. Louis, MO), nylon 6,6 (Sigma Aldrich, St. Louis, MO), and formic acid, 99% (Mallinckrodt, Phillipsburg, NJ) were used as received. Silicon wafers used in the direct deposition of **1** were 5", P type, <1-0-0>, 0.01-0.02 ohm-cm, 605-645 μm, single side polished epi wafers (WRS Materials, San Jose, CA). Silicon wafers used for spin coating of nylon films and subsequent deposition of **1** were 2", P type, <1-0-0>, 0-100 ohm-cm, 280 μm, test grade (University Wafer, South Boston, MA).

4.3.2 Deposition of **1**

Alternating deposition of **1** and either water or aqueous ammonium hydroxide in a molecular layer deposition (MLD)-like fashion was performed in a YES 1224P deposition system (Yield Engineering Systems, Livermore, CA). The ammonia in aqueous NH_4OH is believed to act as a catalyst for hydrolysis of the methoxy groups in **1**. The oven temperature was 55 °C, *many consumer electronic devices will not withstand higher temperatures for significant amounts of time*, and the vapor flasks were set at 80 °C. Samples were first plasma treated in the 1224P with oxygen and hydrogen plasmas for 60 s each at 0.5 Torr base pressure with a flow rate of 20 sccm

for each gas. The active plate was at the highest available position in the chamber, the ground plate was 2 cm below the active plate (at the next available position in the chamber), and the float plate was located 4 cm (two positions) below the ground plate. Samples were placed on the float plate, where there should be essentially no oxidation of the material during plasma treatment, only cleaning.[23] After plasma treatment, thicknesses were measured ex situ using spectroscopic ellipsometry (SE) and these thicknesses were used as the initial thicknesses of the silica (native oxide) or of the spin coated nylon films to determine subsequent film growth.

After ellipsometry, the samples were returned to their positions on the float plate and the system was pumped down to 0.5 Torr. At this base pressure, 0.3 ml of **1** was injected into a vapor flask and the resulting vapors were introduced into the deposition chamber for 10 min. After evacuation for 5 min, the base pressure was again achieved, which was followed by injection of 1 ml of water or ammonium hydroxide into a different vapor flask and the exposure of the surface to these vapors for 10 min. After completion of one AB cycle, i.e., exposure to **1** (A), followed by exposure to water or ammonium hydroxide (B), the system was purged three times with dry nitrogen before the cycle was repeated. This 'AB' sequence was repeated different numbers of times to grow barrier layers of different thicknesses.

4.3.3 Spin coating of nylon

A 1% solution of a 1:1 mixture of nylon 6,6 and nylon 6 in formic acid was used for spin coating nylon onto silicon wafers. Accordingly, a 2" silicon wafer was first air plasma treated for 120 s in a plasma cleaner (PDC-32 G, Harrick Plasma, Ithaca, NY). Plasma-treated silicon wafers were then placed on the chuck of a spin coater ((WS-400B-6NPP/LITE, Laurell Technologies

Corporation, North Wales, PA), covered/wetted with an excess of solution, and spun at 3,000 rpm for 30 s.

4.3.4 Deposition of a hydrophobic layer

A hydrophobic film of (tridecafluoro-1,1,2,2-tetrahydrooctyl)trimethoxysilane (F-13 silane) (Gelest, Morrisville, PA) was deposited by chemical vapor deposition onto barrier layers of **1**. That is, thin films of **1** were placed in a home-built chemical vapor deposition oven, the oven was pumped down to 1 Torr (the base pressure) followed by injection of 0.3 mL of ammonium hydroxide. The oven temperature was 55 °C. Ammonium hydroxide appears to serve to: (i) complete any remaining crosslinking of the underlying barrier layer of **1**, and (ii) facilitate subsequent bonding of the F-13 silane to itself and the layer of **1**. After the vapors of NH_4OH had sat in the chamber for 10 min., and without evacuating the chamber, 0.2 mL of the F-13 silane was injected into the oven and allowed to react in vapor form with the surface for 10 min. The chamber was then purged three times with dry nitrogen.

4.3.5 Ellipsometric Thickness

Thicknesses were measured with an M-2000 ellipsometer (J.A. Woollam, Co. Lincoln, NE). Measurements were taken at an incidence angle of 75°, which is near the Brewster angle for silicon. At the Brewster angle of a material, no p-polarized light is reflected, which leads to enhanced sensitivity for the ellipsometric measurement. The wavelength range was 200 – 1000 nm, although for nylon-on-silicon films, the data were range selected from 600 to 1000 nm in the analysis. The experimental data for bare silicon wafers were fitted to an air/SiO_2/Si model, and the optical constants of silica (SiO_2.jaw) and silicon (Si.jaw) were taken from the instrument software. Using this model and these optical constants, the thickness of the silicon native oxide

layer was found to be ca. 1.8 nm, which varied slightly from sample to sample. For spin-coated nylon samples, a model consisting of air/Cauchy layer/SiO$_2$/Si was used. In this model, the thickness/optical constants of the SiO$_2$ native oxide layer and Si substrate layers had previously been determined and were fixed, so the only unknowns were the film thickness and the A, B, and C parameters of the Cauchy layer, which has k = 0 over all wavelengths and:

$$n(\lambda) = A + B/\lambda^2 + C/\lambda^4 \tag{1}$$

These models gave reasonably small MSE (error) values and very reproducible results.

4.3.6 Surface Characterization

Water contact angles were measured with a Model 100-00 contact angle goniometer from Ramé-Hart (Netcong, NJ) that was fitted with a syringe filled with high purity water. X-ray photoelectron spectroscopy (XPS) was performed on different thicknesses of the barrier layer prepared from **1** using a Surface Science SSX-100 X-ray photoelectron spectrometer (serviced by Service Physics, Bend, OR) with a monochromatic Al K$_\alpha$ source, a hemispherical analyzer, and a take-off angle of 35°. Survey scans were recorded with an 800 μm x 800 μm spot and a resolution of 4. Narrow scans were recorded with a 200 μm x 200 μm spot and a resolution of 2. A flood gun for charge compensation was operated at 4 eV and peaks were referenced to the C 1s hydrocarbon signal at 284.6 eV. Atomic force microscopy (AFM) was performed in tapping mode on barrier layers using a Dimension 3100 AFM (Veeco, Plainview, NY) using a tip with an Al reflective coating (OTESPA, 42 N/m, 300kHz, Bruker, Madison, WI) over a 5 μm x 5 μm area with a height scale of 25 nm. Time-of-flight secondary ion mass spectrometry (ToF-SIMS) was performed with an ION-TOF (Münster, Germany) TOF-SIMS IV instrument

with monoisotopic 25 keV ^{69}Ga$^+$ primary ions in "bunched mode." The primary ion (target) current was typically 1.8 μA, with a pulse width of 20 ns before bunching. The raster area of the beam was 100 × 100 μm^2.

4.3.7 Water Immersion Test

Specially designed circuits containing two interdigiated electrodes that were separated by a small gap and which made them non-conductive initially, were used for these tests. The circuits were then able to conduct when immersed in a solution of an electrolyte (tap water). After immersion, the voltage was ramped from 0 V to 8 V in 2 min. The amount of current across the electrodes was used as a quantitative measure of the effectiveness of the barrier layer over them.

4.4 Results and Discussion

*4.4.1 Overview of MLD-like deposition of N-n-butyl-aza-2,2-dimethoxysilacyclopentane, **1**, and water*

It was believed that deposition of **1** and water would follow an MLD-like process,[19] with **1** reacting with silanol groups on silica, followed by hydrolysis (and perhaps) condensation of the methoxy groups on **1**, and more **1** reacting with silanol groups in the film (see Figure 4.2). Interestingly, repeated deposition of **1** and water (or ammonium hydroxide) led to the expected film growth for the first few cycles, but ultimately appeared to reduce the number of reactive sites so that self-termination of the process occurred.

*4.4.2 Alternating deposition of **1** and H$_2$O on Si/SiO$_2$.*

The deposition of bilayers of **1** and water on Si/SiO2 was monitored ex situ by SE, XPS, wetting, AFM, and ToF-SIMS. In this case, XPS is a particularly useful analysis tool because of the

presence of the nitrogen heteroatom, which is unique to the deposition of **1** and gives chemical specificity to the analysis. XPS survey spectra of films of **1** on Si/SiO$_2$ show only the elements expected: Si, C, O, and N. The XPS C 1s narrow scan suggested carbon bonded to oxygen or nitrogen (relatively small chemical shifts), but no signals that might be attributed to carbonyl, carboxyl, or aromatic (shake-up peak) carbon.

All of the characterization techniques yielded data that were consistent with significant growth of the film initially; film growth appeared to proceed in a roughly linear fashion for the first four cycles leading to a film thickness of ca. 2.3 nm, an N/Si ratio by XPS of ca. 0.2, and a modest increase in film roughness to ca. 0.7 nm (see Figure 4.3). AFM imaging at different spots on the surfaces suggested complete, pin-hole free coverage of films of **1**. Contact angles, which are very surface sensitive, were nearly the same for all films made with 2 – 10 bilayers of **1** and water and showed the films to be moderately hydrophobic ($\theta_a \sim 75°$), suggesting that a similar chemistry and no significant increase in roughness is present at the film-air interfaces of the surfaces probed. Negative ion ToF- SIMS of films with 2 – 10 bilayers of **1** and water showed a signal from CN$^-$, which is typical of nitrogen-containing organic materials.[22] This peak was not present on the uncoated surfaces.

Linear fits (dashed lines) to the first three data points (0, 2, and 4 cycles) in the plots of the SE, XPS, and AFM results are shown in Figure 4.3. The fits for the SE and XPS data were constrained to pass through the origin (y = mx), while the fit to the AFM data was not (y = mx + b), although (analogous to the SE and XPS data) its y-intercept turned out to have almost the same value as the first point. In all cases, the first part of the film growth with **1** and H$_2$O is

approximately linear, although in each case, the data point corresponding to two cycles is above the fit line and the data point at four cycles is below it, suggesting curvature in the data and a slowing of the growth. That the film growth is not continuing in a linear fashion is shown clearly at six cycles, where the difference between the linear fit lines and data points becomes noticeable. As the number of cycles continues, this deviation becomes extreme, and growth appears to stop altogether. Given the highly reactive nature of **1**, these results suggest that the number of reactive sites in the films is decreasing with film growth. The overall SE, XPS and AFM data in Figure 4.3 could be fit quite well to an empirical function of the form $y = a(1-e^{-bx}) +$ offset, which is consistent with an asymptotic/self-terminating/controllable deposition of the film.

4.4.3 Alternating deposition of **1** and NH$_4$OH on Si/SiO$_2$

It was of interest to know whether the presence of a catalyst in the gas phase (NH$_3$) would allow continued growth of **1** to take place, or whether it might more quickly induce the self-limiting behavior seen in the growth of **1** and H$_2$O. This approach seemed reasonable because ammonium hydroxide and amines have previously been used as catalysts for liquid-phase silane deposition,[21, 24, 25] and various amines, but to the best of our knowledge not ammonia, have similarly been used to catalyze the gas-phase deposition of silanes.[25-27] Thus, the presence of NH$_3$ from ammonium hydroxide would be expected to accelerate the hydrolysis of the methoxy groups in films of **1**. Figure 4.4 shows the characterization of films of **1** and NH$_4$OH on Si/SiO$_2$ by SE and wetting. Interestingly, the effects previously shown in the deposition of **1** and H$_2$O on Si/SiO$_2$ (Figure 4.3) seem to be accelerated, i.e., the films terminate faster – to a thickness of ca. 1.5 nm instead of ca. 2.5 nm. This result would be consistent with a decreased number of active

sites in the growing films as a result of an increased degree of hydrolysis and crosslinking

between chemisorbed molecules of **1**. The contact angles of surfaces prepared from **1** and
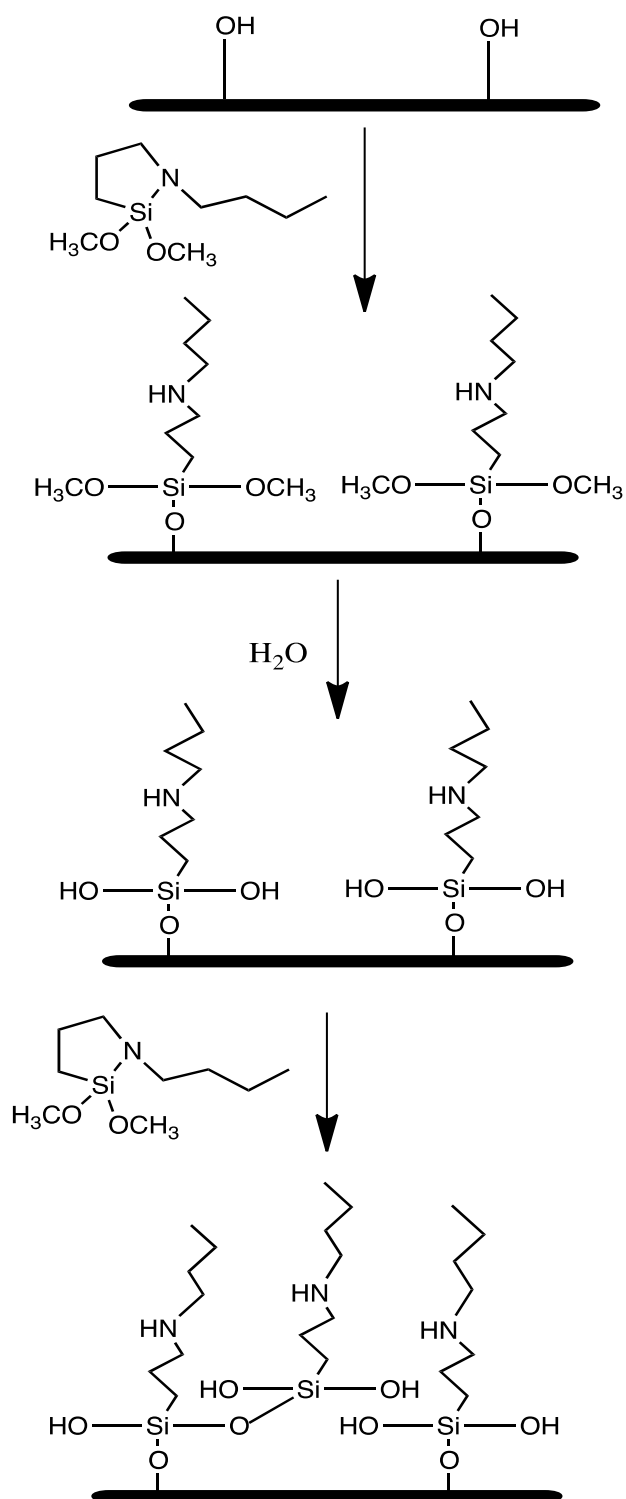
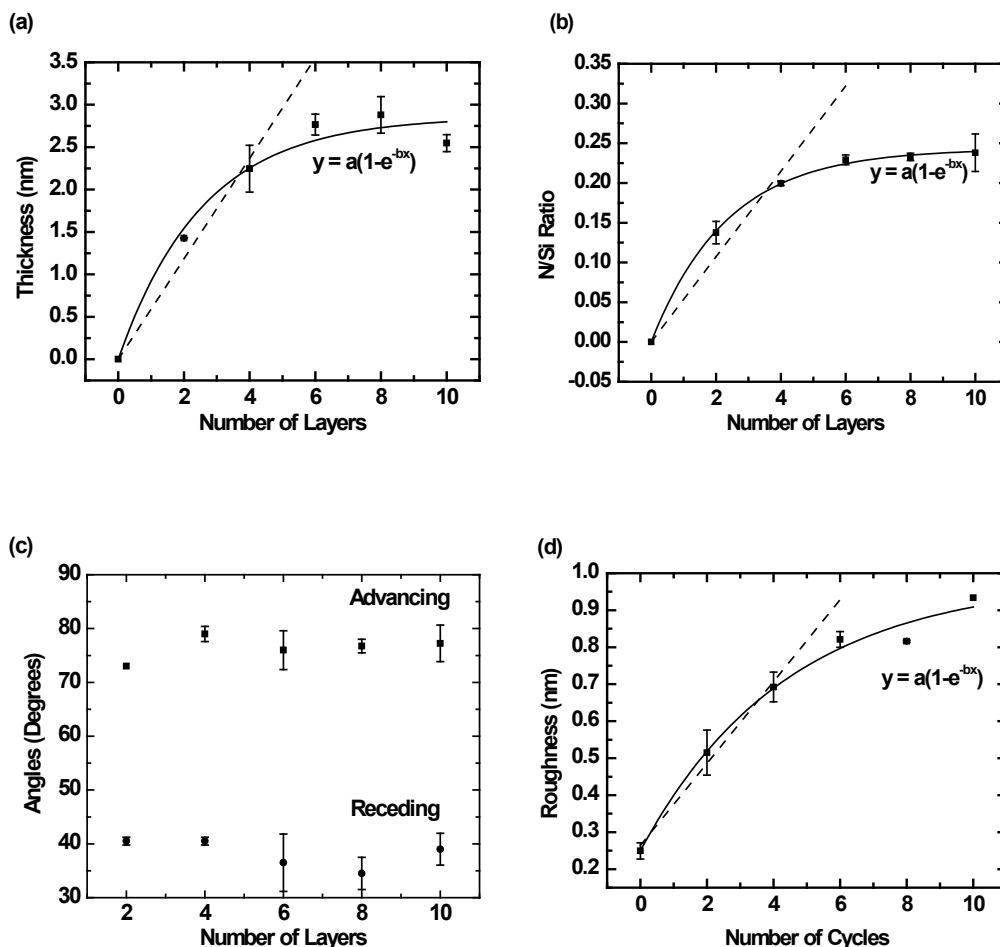Figure 4.2 Possible growth mechanism of N-n-butyl-aza-2,2-dimethoxysilacyclopentane, 1, and water on Si/SiO$_2$.

Figure 4.3 Characterization of films of **1** and water on Si/SiO$_2$ as a function of the number of deposition cycles by (a) Spectroscopic ellipsometry, with the resulting thicknesses fitted to an empirical function of the form: $y = a(1-e^{-bx})$ + offset (offset = 0), a = 2.9 $\pm$ 0.2 and b = 0.4 $\pm$ 0.08 with R^2 = 0.98, and the first three points fit to y = mx with m= 0.60 and R^2 = 0.99; (b) XPS, with the data (the N/Si ratio) fitted to the same function as above (offset = 0): a = 0.242 $\pm$ 0.002 and b = 0.43 $\pm$ 0.02 with R^2 = 0.995, and the first three points fit to y = mx with m = 0.54 and R^2 = 0.98; (c) Contact angle goniometry (advancing and receding water contact angles); and (d) AFM with the resulting roughnesses fitted to the same type of function as above (offset = 0.25), a = 0.73 $\pm$ 0.05 and b = 0.23 $\pm$ 0.04 with R^2 = 0.99, and the first three points fit to y = mx + b with m = 0.11, b = 0.26, and R^2 = 0.99.
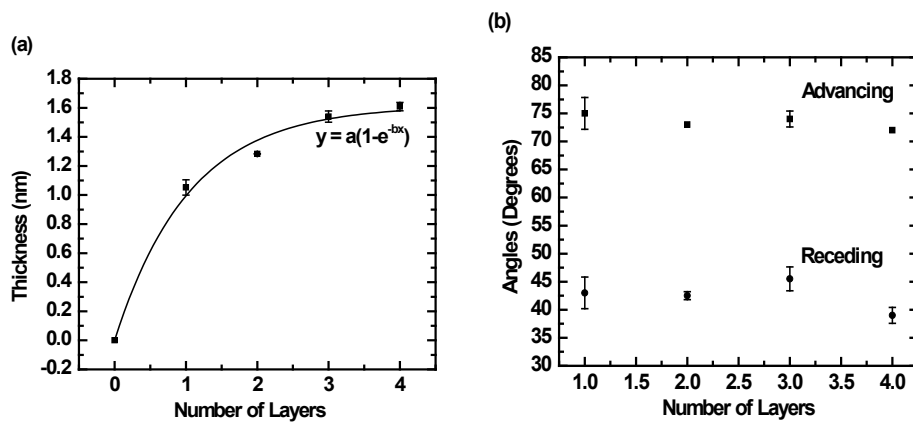
Figure 4.4 Characterization of films of **1** and NH_4OH on Si/SiO_2 substrates as a function of the number of deposition cycles by (a) spectroscopic ellipsometry (data fit to the function $y = a(1-e^{-bx})$, a = 1.61 $\pm$ 0.07 and b = 0.96 $\pm$ 0.14 with R^2 = 0.992), and (b) wetting (advancing and receding water contact angles).

NH$_4$OH are essentially the same as those prepared from **1** and H$_2$O (see Figures 4.3 and 4.4), suggesting that all the films share a similar chemistry. Thus, the choice of the half-reactant (H$_2$O or NH$_4$OH) in the deposition of **1** can be used to control film thickness.

*4.4.4 Alternating deposition of **1** and H$_2$O on nylon*

Thin film deposition onto both inorganic *and* organic substrates, especially polymeric materials, is of technological interest. Accordingly, deposition of **1** was studied on spin-coated nylon substrates that had undergone the same plasma treatment as the Si/SiO$_2$ substrates used above – the majority of the nylon film was still present after the plasma treatment, where Si/SiO$_2$ and Si/SiO$_2$/nylon substrates were positioned side by side in the chamber during deposition of **1** and H$_2$O or NH$_4$OH. Figure 4.5 shows SE and wetting characterization of film growth of **1** and water on nylon. There are two immediate and obvious differences between these results and the comparable results on the Si/SiO$_2$ substrate (Figure 4.3). The first is that a much thicker film is deposited on nylon than on Si/SiO$_2$. While after 10 cycles the film of **1** and H$_2$O on Si/SiO$_2$ was approximately 2.5 nm, the film thickness of **1** and H$_2$O on the nylon substrate is greater than 30 nm. A second difference is that while film growth appears to be slowing, it does not appear to have reached an asymptote after 10 cycles on the nylon substrate. Advancing water contact angles of the **1**/H$_2$O films on the two substrates are similar – they are only a few (ca. 5) degrees higher on the nylon substrate. Receding water contact angles on the two substrates are also quite similar. We have previously reported that a nylon film can act as a reservoir of water in deposition of a fluorosilane film, where this water acts as a reactant in silane condensation and film growth.[28] We again attribute the significantly greater film thickness of **1** and H$_2$O on nylon to this effect.

*4.4.5 Alternating deposition of **1** and NH₄OH on nylon*

Deposition of **1** and NH$_4$OH (compared to H$_2$O) on nylon followed the same trend as deposition

of these species on Si/SiO$_2$. That is, the presence of the catalyst again limited film growth (this

time to ca. 13 nm), although this time there was much more evidence for self-termination of the

film. These results can again be explained by a model of increased hydrolysis of methoxy groups

on **1**, followed by condensation of the resulting silanols, leading to fewer available reactive sites
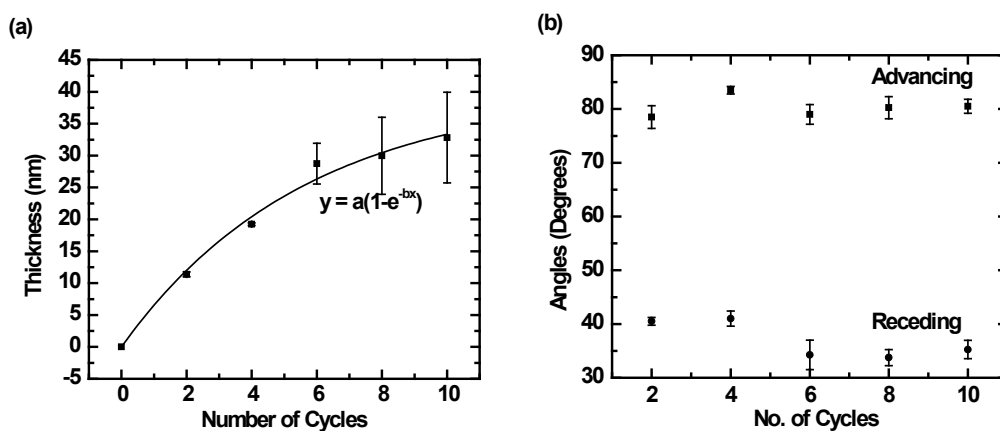

Figure 4.5 Characterization of films of **1** and H$_2$O on nylon substrates as a function of number of deposition cycles by (a) spectroscopic ellipsometry (data fit to the function y = a(1-e^{-bx}), a = 40.1 ± 3.9 and b = 0.18 ± 0.03 with R^2 = 0.99), and (b) wetting (advancing and receding water contact angles).
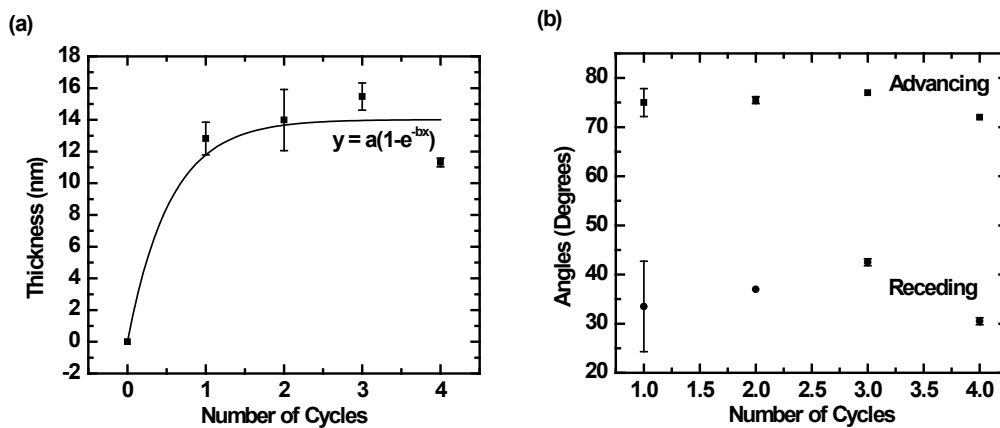
(a)

(b)

Figure 4.6 Characterization of films of **1** and NH$_4$OH on nylon substrates as a function of the number of deposition cycles by (a) spectroscopic ellipsometry (data fit to the function $y = a(1-e^{-bx})$, a = 14.0 $\pm$ 0.8 and b = 1.84 $\pm$ 0.00 with R^2 = 0.93), and (b) wetting (advancing and receding water contact angles).

on the surface, and ultimately termination of film growth. Advancing and receding water contact angles on these films were again similar to those found on all films of **1** reported in this work.

*4.4.6 Alternating deposition of **1** and H$_2$O as a barrier layer on a test circuit*

A film of **1** and H$_2$O, with a fluorosilane deposited on top of it for added hydrophobicity, was deposited on a test circuit to determine whether the film would show water-resistive properties. The quality of the film would be determined based on the amount of current that would pass when the circuit was immersed in water – the less current the better. As expected, control circuits coated only with the fluorosilane showed higher currents than the other films (see Figure 4.7), which were coated with **1**/H$_2$O followed by the fluorosilane. Also as expected, 4 cycles of **1**/H$_2$O + fluorosilane proved to be a better barrier layer than 2 cycles of **1**/H$_2$O + fluorosilane. These results are consistent with films of **1**/H$_2$O showing some ability to act as a barrier against water.
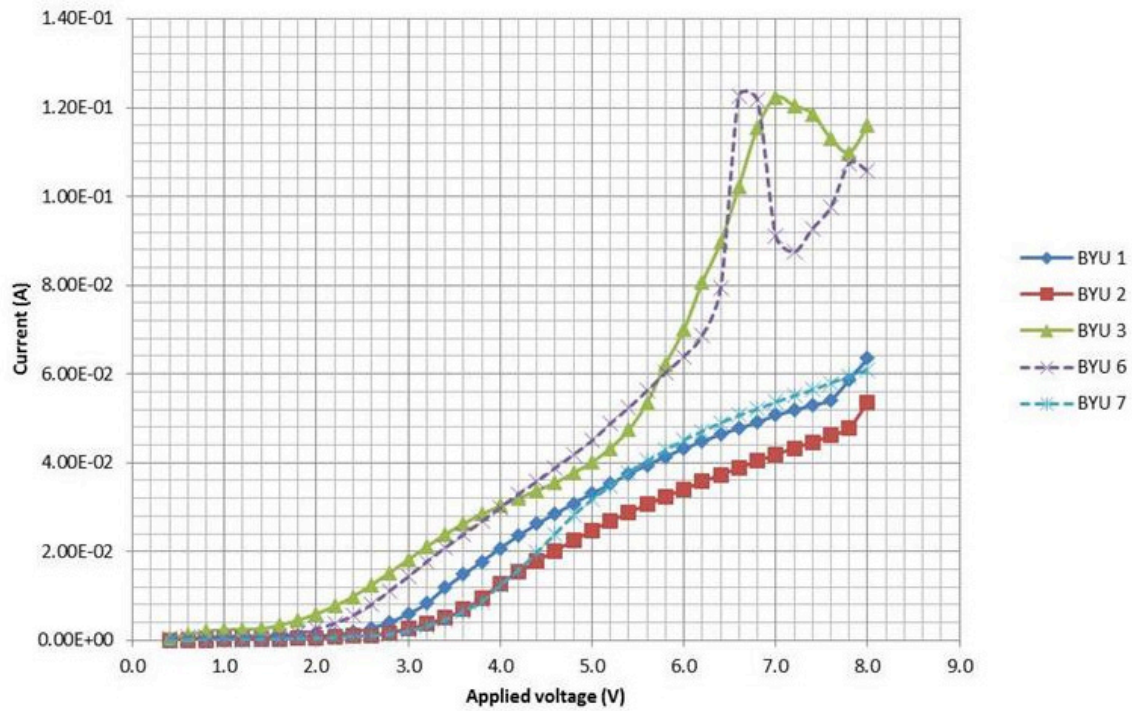
4.5 Acknowledgment

Figure 4.7 Water Immersion test on specially designed circuits coated with different numbers of barrier layers of **1** and H_2O and a fluorosilane. The BYU 3 and BYU 6 coatings are just the fluorosilane, BYU 1 and BYU 7 consist of two cycles of **1** and H2O followed by the fluorosilane, and BYU 2 consists of four cycles of **1** and H_2O followed by the fluorosilane.

4.6 REFERENCES

1.   Mark A. Roehrig, A. K. N., Mark D. Weigel Moisture Resistance Coating for Barrier Films. 2012.

2.   Kim, Y.-H.; Moon, D.-G.; Han, J.-I., Organic TFT array on a paper substrate. *Electron Device Letters, IEEE* **2004,** 25, (10), 702-704.

3.   Chen, T.-N.; Wuu, D.-S.; Wu, C.-C.; Chiang, C.-C.; Chen, Y.-P.; Horng, R.-H., Improvements of Permeation Barrier Coatings Using Encapsulated Parylene Interlayers for Flexible Electronic Applications. *Plasma Processes and Polymers* **2007,** 4, (2), 180-185.

4.   Egert, C. M. Protective coatings for sensitive materials. 5654084, 1997.

5.   Xing Yang, C. G., And Yu-Chong Tai, A Low Power MEMS Silicone/Paralyne Valve. In *Solid-State sensor and Actuator Workshop*, Hilton Head Island, SC 1998.

6.   Stephen D. Pacetti, S. F. A. H. Diffusion Barrier Layer for Implantable Devices. 6663662 B2, 2003.

7.   Damein C. Rodger, J. D. W., Mark S. Humayun, Yu-Chong Tai, Scalable high lead-count parylene package for retinal prostheses. *Sensors and Actuators B* **2006,** 117, 107-114.

8.   Metroke, T. L.; Parkhill, R. L.; Knobbe, E. T., Passivation of metal alloys using sol–gel-derived materials — a review. *Progress in Organic Coatings* **2001,** 41, (4), 233-238.

9.   Gray, J. E.; Luan, B., Protective coatings on magnesium and its alloys — a critical review. *Journal of Alloys and Compounds* **2002,** 336, (1–2), 88-113.

10.   Lange, J.; Wyser, Y., Recent innovations in barrier technologies for plastic packaging—a review. *Packaging Technology and Science* **2003,** 16, (4), 149-158.

11.   Erlat, A. G.; Henry, B. M.; Grovenor, C. R. M.; Briggs, A. G. D.; Chater, R. J.; Tsukahara, Y., Mechanism of Water Vapor Transport through PET/AlOxNy Gas Barrier Films. *The Journal of Physical Chemistry B* **2003,** 108, (3), 883-890.

12.   Deng, C. S.; Assender, H. E.; Dinelli, F.; Kolosov, O. V.; Briggs, G. A. D.; Miyamoto, T.; Tsukahara, Y., Nucleation and growth of gas barrier aluminium oxide on surfaces of poly(ethylene terephthalate) and polypropylene: effects of the polymer surface properties. *Journal of Polymer Science Part B: Polymer Physics* **2000,** 38, (23), 3151-3162.

13.   Yang, Y.; Kim, K.-H.; Ong, J. L., A review on calcium phosphate coatings produced using a sputtering process—an alternative to plasma spraying. *Biomaterials* **2005,** 26, (3), 327-337.

14.   Yong-Hoon, K.; Dae-Gyu, M.; Jeong-In, H., Organic TFT array on a paper substrate. *Electron Device Letters, IEEE* **2004,** 25, (10), 702-704.

15.   Haas, K.-H.; Amberg-Schwab, S.; Rose, K., Functionalized coating materials based on inorganic-organic polymers. *Thin Solid Films* **1999,** 351, (1–2), 198-203.

16.   Haas, K.-H.; Wolter, H., Synthesis, properties and applications of inorganic–organic copolymers (ORMOCER®s). *Current Opinion in Solid State and Materials Science* **1999,** 4, (6), 571-580.

17.   Amberg-Schwab, S.; Katschorek, H.; Weber, U.; Burger, A.; Hänsel, R.; Steinbrecher, B.; Harzer, D., Inorganic-Organic Polymers as Migration Barriers Against Liquid and Volatile Compounds. *Journal of Sol-Gel Science and Technology* **2003,** 26, (1), 699-703.

18.   Messaddeq, S. H.; Pulcinelli, S. H.; Santilli, C. V.; Guastaldi, A. C.; Messaddeq, Y., Microstructure and corrosion resistance of inorganic–organic (ZrO2–PMMA) hybrid coating on stainless steel. *Journal of Non-Crystalline Solids* **1999,** 247, (1–3), 164-170.

19.   George, S. M.; Yoon, B.; Dameron, A. A., Surface Chemistry for Molecular Layer Deposition of Organic and Hybrid Organic–Inorganic Polymers. *Accounts of Chemical Research* **2009,** 42, (4), 498-508.

20.   Yoshimura, T.; Tatsuura, S.; Sotoyama, W., Polymer films formed with monolayer growth steps by molecular layer deposition. *Applied Physics Letters* **1991,** 59, (4), 482-484.

21.   Blitz, J. P.; Shreedhara Murthy, R. S.; Leyden, D. E., The role of amine structure on catalytic activity for silylation reactions with Cab-O-Sil. *Journal of Colloid and Interface Science* **1988,** 126, (2), 387-392.

22.   Saini, G.; Gates, R.; Asplund, M. C.; Blair, S.; Attavar, S.; Linford, M. R., Directing polyallylamine adsorption on microlens array patterned silicon for microarray fabrication. *Lab on a Chip* **2009,** 9, (12), 1789-1796.

23.   Zhang, F.; Sautter, K.; Davis, R. C.; Linford, M. R., Subsurface Oxidation for Micropatterning Silicon (SOMS). *Langmuir* **2009,** 25, (3), 1289-1291.

24.   Blitz, J. P.; Murthy, R. S. S.; Leyden, D. E., Ammonia-catalyzed silylation reactions of Cab-O-Sil with methoxymethylsilanes. *Journal of the American Chemical Society* **1987,** 109, (23), 7141-7145.

25.   White, L. D.; Tripp, C. P., Reaction of (3-Aminopropyl)dimethylethoxysilane with Amine Catalysts on Silica Surfaces. *Journal of Colloid and Interface Science* **2000,** 232, (2), 400-407.

26.   Kanan, S. M.; Tze, W. T. Y.; Tripp, C. P., Method to Double the Surface Concentration and Control the Orientation of Adsorbed (3-Aminopropyl)dimethylethoxysilane on Silica Powders and Glass Slides. *Langmuir* **2002,** 18, (17), 6623-6627.

27.   L.D. White, C. P. T., An infrared Study of the Amine-Catalyzed Reaction of Methoxymethylsilanes with Silica. *Journal of Colloid and Interface Sciences* **2000,** 227, 237-243.

28.   Saini, G.; Sautter, K.; Hild, F. E.; Pauley, J.; Linford, M. R., Two-silane chemical vapor deposition treatment of polymer (nylon) and oxide surfaces that yields hydrophobic (and superhydrophobic), abrasion-resistant thin films. *Journal of Vacuum Science & Technology A: Vacuum, Surfaces, and Films* **2008,** 26, (5), 1224-1234.

Chapter 5 Data and Device Protection: A ToF-SIMS, Wetting, and XPS Study of an Apple iPod Nano

5.1 Introduction

Many people have digital pictures, family movies, and other documents of importance that they wish to pass on to their posterity. Long-term data storage is an important topic for these consumers. For the past few years some of us have worked actively in this area, developing a durable DVD[1] that is now sold commercially by Millenniata[TM] as the 'M-DISC'.

An important aspect of data longevity is exposure to water, dirt, fingerprints, and smudges that may compromise the integrity of the information within a device and/or its ability to function. Accordingly, hydrophobic and oleophobic coatings have been applied to various consumer electronic devices to protect them. Here we report a ToF-SIMS, wetting, and XPS study of an Apple iPod nano device that shows a protective coating on its touchscreen, but interestingly not on other parts of the device. SIMS, in particular, suggests the use of a fluorinated coating with oxygen in it.

ToF-SIMS, wetting, and XPS were performed as described previously,[2] where the SIMS negative ion spectra were calibrated to the H^-, C^-, CH_2^-, O^-, F^-, and $C_3F_7O^-$ peaks. A fine nickel mesh was placed just over the surfaces to help reduce charging. XPS and SIMS were performed on all parts of commercially obtained Apple iPod nano devices (8 GB, MC525LL/A) shown in Figure 1, which were cut into pieces prior to analysis so that each analysis could be performed on a fresh, unanalyzed piece of the device. The nanos showed good resistance to their environments– they played continuously while immersed under 6" of water for ca. two hours

Figure 5.1 Images of an Apple iPod nano. (a) touchscreen, (b) back cover, (c) clip, (d) metal sheet, (e) circuit, and (f) circuit

Table 5.1 Advancing and Receding water and hexadecane (HD) contact angles. The first entry in each cell comes from one iPod and the second from a different device. 'y' or 'n' signifies whether roll-off of the probe droplet occurred.

Part	$\theta_a(H_2O)$	$\theta_r(H_2O)$	$\theta_a(HD)$	$\theta_r(HD)$
Touchscreen	121, 121	99, 104 (y)	62, 66	61, 61 (y)
Back Cover	96, 99	60, 62 (n)	8, 8	5, 4 (n)
Clip	103, 112	60, 65 (n)	18, 22	7, 9 (n)
Metal Sheet	78, 86	39, 35 (n)	22, 15	9, 9 (n)

before failing. The coating on the touchscreen appears to be important for device function. When it was removed/altered by plasma treatment, the device only survives ca. 30 min while playing under 6" of water.

5.2 Results and Discussion

Table 1 gives the advancing and receding contact angles of water and hexadecane on the nano. The touchscreen is obviously the most hydrophobic and oleophobic region, showing high advancing and receding water and hexadecane contact angles. This is also the only spot on the device where there is 'roll-off' of water and hexadecane drops, i.e., where these liquids will roll off the surface when it is tilted.

Fluorinated hydrocarbons provide one way of lowering surface free energies and obtaining hydrophobic and oleophobic materials. Accordingly, various areas on the iPod were probed by XPS to determine whether a fluorinated material was responsible for the high water contact angles observed on the device, especially on the touchscreen. XPS is a reasonable technique for probing for fluorine; XPS is ca. four times more sensitive to fluorine than to carbon. Interestingly, the touchscreen is the only part of the device that shows an intense fluorine signal (Figure 2a). Other regions showed little or no F (see Figure 2b and area ratios in its caption). The C 1s narrow scan from the touchscreen is consistent with a fluorinated hydrocarbon, as evidenced by the peak at higher binding energy that is separated by ca. 7 eV from the other carbon peak.[3] None of the other C 1s narrow scans from other parts of the device showed chemically shifted peaks that are consistent with fluorinated carbon. As expected, the narrow F 1s scan from the touchscreen showed a single, Gaussian-like peak. Small signals from Si and Al
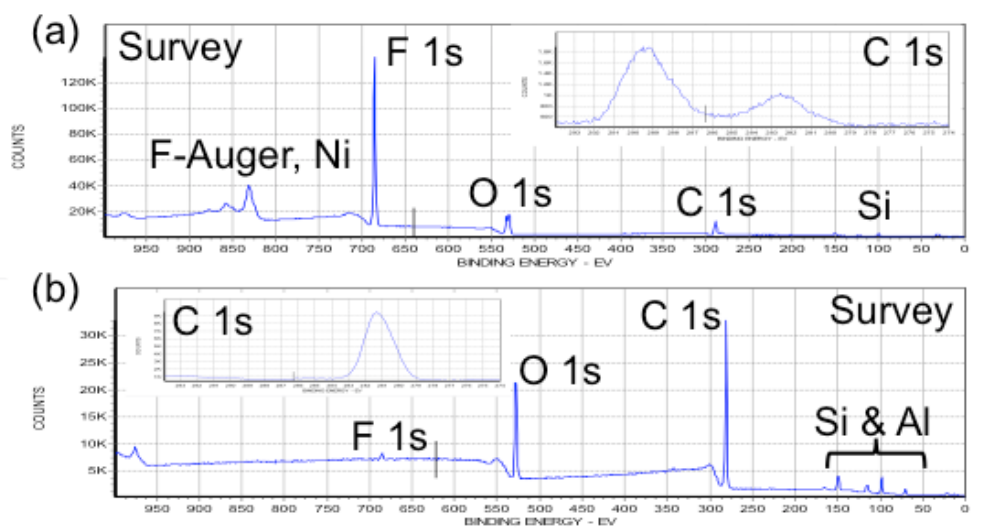
Figure 5.2 XPS spectra of (a) touchscreen, F1s/C1s area ratio: 2.58, and (b) back cover, F1s/C1s area ratio: 0.01. Insets show C 1s spectra.

were observed in all of the survey spectra from all parts of the device, except the touchscreen, which showed only Si.

Both positive and negative ion SIMS were also performed on the nano. The positive ion spectrum of the touchscreen showed a series of intense peaks, all with roughly equal intensities, corresponding to CF^+, CF_3^+, $C_2F_4^+$, $C_2F_5^+$, and $C_3F_7^+$. This set of peaks provides an additional and compelling confirmation of the presence of a fluoropolymer on the touchscreen. In the negative ion mode, the touchscreen showed an intense F^- signal that dominated the low-mass region of the spectrum. Interestingly, a series of peaks containing C, F, and O also appeared to be present, including $C_3O_2F_5^-$, $C_3OF_7^-$, $C_5O_2F_{10}^-$, $C_5O_2F_{11}^-$, $C_6O_3F_{11}^-$, $C_6O_2F_{12}^-$, and $C_6O_2F_{13}^-$. Other regions of the nano showed very little fluorine – the low-mass regions of their negative ion spectra were typically dominated by H^-, with a few other small signals due to CH^-, O^-, and OH^-. These observations are consistent with XPS, i.e., that a fluoropolymer is present on the touchscreen and not on other parts of the device.

The SIMS spectra from the touchscreen were compared to those from an ultrathin (ca. 0.8 nm) film of a fluorinated silane: $(CH_3O)_3SiCH_2CH_2(CF_2)_5CF_3$. In the positive ion spectrum of this silane film, four peaks of roughly equal intensity: Si^+, CF^+, CF_2^+, and CF_3^+, dominated the low-mass region of the spectrum. Note that while the CF_2^+ peak was also present in the spectrum of the touchscreen, its intensity was noticeably lower than the intensities of the CF^+ and CF_3^+ peaks. An addition difference between the positive ion spectra of the touchscreen and silane film is that only low intensity $C_2F_4^+$, $C_2F_5^+$, and $C_3F_7^+$ signals were produced by the fluorinated silane film. Even more dramatic differences were observed in the negative ion spectrum of the silane

monolayer. To wit, it showed none of the oxygen-containing negative ions produced by the touchscreen. A general principle of SIMS is that molecular fragments produced by the technique generally come from atoms that were bonded together in the material. Thus, these spectral differences suggest that the fluorinated film on the nano touchscreen consists of segments of fluorinated carbons interspersed with oxygen atoms, perhaps via ether linkages. Such oxygen may improve the biodegradability of the films. It may also help in cationization in SIMS, leading to the heavier fluorocarbon ions observed from the touchscreen.

5.3 Conclusions

To protect their device, Apple coats the front panel of their iPod nano with a fluorocarbon polymer. Interestingly, no other part of the device has this coating.

5.4 Acknowledgment

5.5 References

1. Jonathan Abbott, Travis L. Niederhauser, Douglas P. Hansen, Raymond T. Perkins, David A. Bell, Erik C. Bard, Barry M. Lunt, Mark O. Worthington, C. Michael Miller, Daniel F. Hyatt, Matthew C. Asplund, Guilin Jiang, Matthew R. Linford, Richard R. Vanfleet and Robert C. Davis, ACS Applied Materials and Interfaces **2010**, 2(8), 2373 -2376.

2. Saini, Sautter, Hild, Pauley, Linford J. Vac. Sci. Technol. A. **2008**, 26(5), 1224–1234.

3. Ferraria, da Silva, Botelho do Rego Polymer **2003**, 44, 7241–7249.

Chapter 6 Conclusions and Future Work

My work on validating the Calzaferri suggestion for assigning oxidation states to organic molecules using a well-documented and well-known core-electron spectroscopy (XPS), reemphasizes the importance of his work. I hope this study will encourage more chemists to use his suggestion, particularly in their teaching. Indeed, the Calzaferri approach should allow the greater application of oxidation numbers to organic and biological reactions. I further hope this work will inspire others to employ other analytical techniques to resolve/elucidate other underlying concepts of chemistry. Throughout my work I have tried to explore some of the many possible applications of XPS and other surface analytical techniques; I hope XPS will continue to be applied in non-traditional ways to solve important scientific problems. Similarly ToF-SIMS has played an important role in my work and might find use in other areas of chemistry. For example, the different energies and chemical natures of primary ion beams might be able to differentiate between the different types of bonds in adsorbates, which might later help to elucidate surface structures or to influence the direction of reactions/ syntheses.

My work on introducing a new plasma etch gas for specifically functionalizing the surface to enhance silane loading as an in-situ 'dry' clean, opens up new opportunities for surface scientists. My study shows that glow discharge cleaning can not only be used for effective cleaning of inorganic surfaces, but that it could also be used to specifically functionalize the same, which is an area that does not appear to have been extensively studied. Other etch gases such as ozone, ammonia or specifically synthesized gases might find use for surface oxidation, amination or in other surface modifications, where these modifications will typically be rapid. This approach will

not only save time, money and energy, but it might also lead to more controllable processes and new advances in the field of surface science. I personally feel that in the near future, plasmas will find many uses in various fields of technology, as they intrinsically provide all the basic components of a chemical reaction i.e. both energy and reactants. The one thing that needs to be taken care of at the moment is the control of the resultant chemical reactions, and my work demonstrate the same, i.e., that plasma reactions can be controlled to a significant extent. I hope this work will inspire others to investigate other possible surface or chemical reactions, which could be achieved with the successful use of plasmas.

My work on the deposition of a nano-scale, smooth, conformal, and self limiting multilayers of a hydrophobic barrier film provides a new dimension to hydrophobic coatings, which not only rely on hydrophobicity but also provide a mechanical barrier towards water. These coatings may find applications in various fields, including electronics, semiconductors, microfabrication, etc. This work provides a new stage for coupling two well-known dry deposition process i.e. CVD and ALD/MLD, and hence enjoys the benefits of both, while perhaps overcoming the limitations of each. This work opens up new possibilities of experimenting with different precursor molecules and chemistries to put down a thick, water resistive barrier layer on different substrates. The use of inorganic-organic hybrid molecules allows one to provide a coating with both mechanically and chemically resistance roperties. Both CVD and ALD have been explored to a great extent, but separately. I hope this attempt to unite the two techniques, might bring out some new applications in both the fields.

My work on characterizing the apple iPod nano for its hydrophobic and oleophobic nature has led to the interesting finding that these devices are only coated on their touchscreens and not the other parts of the device, and the coating appears to be prepared from an oxygen-containing fluoropolymer precursor. This characterization study gives a future direction for an effective, biodegradable and an economical hydrophobic coating on electronic devices. This study also demonstrates the usefulness of various surface analytical techniques for investigation of surface coatings and shows how they can complement each other. This study emphasizes the joint capabilities of XPS and ToF-SIMS for structural elucidation of surface coatings. I hope this study will encourage other workers in surface science to exploit the benefits of using multiple techniques to extract the maximum information possible about surfaces and interfaces.

I. Appendix 1

A1.1 Supporting Information for: Chapter 3. Improved Silane Deposition on Hydrogen Plasma-Treated Silicon Dioxide
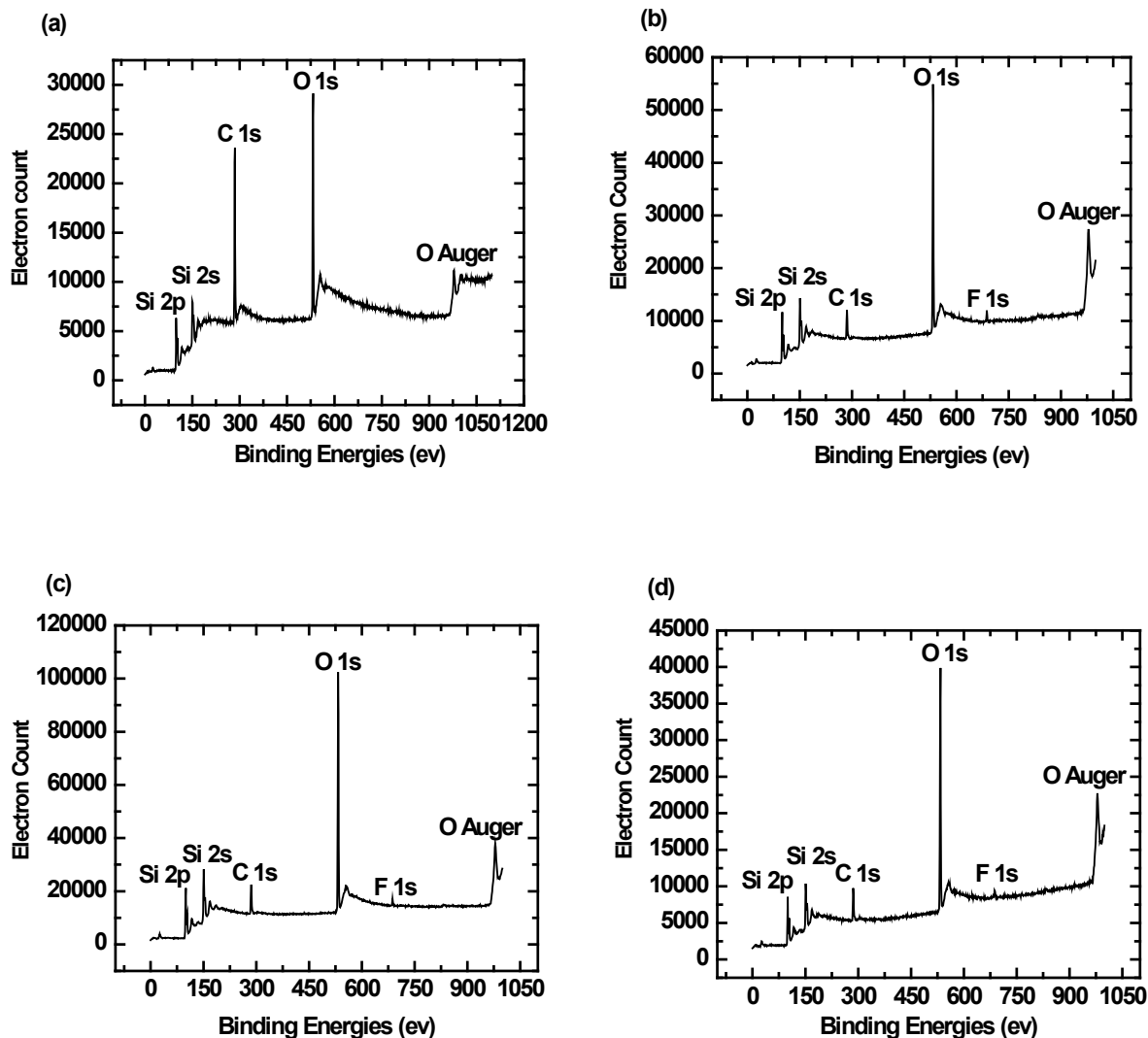

Figure I.1 XPS spectra of Si/SiO$_2$ shards (a) Before plasma treatment (b) After 30 s oxygen plasma treatment (c) After 30 s argon plasma treatment (d) After 30 s hydrogen plasma treatment. These spectra indicate a substantial decrease in the amount of carbon (representative of hydrocarbon contamination) after 30 s plasma treatments with three plasma etch gases. The pump down in our XPS chamber is slow and may introduce hydrocarbon contamination onto clean (high free energy) surfaces. A small amount of fluorine contamination was also seen in a few cases.
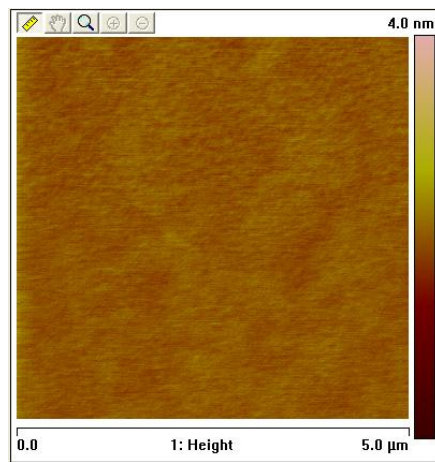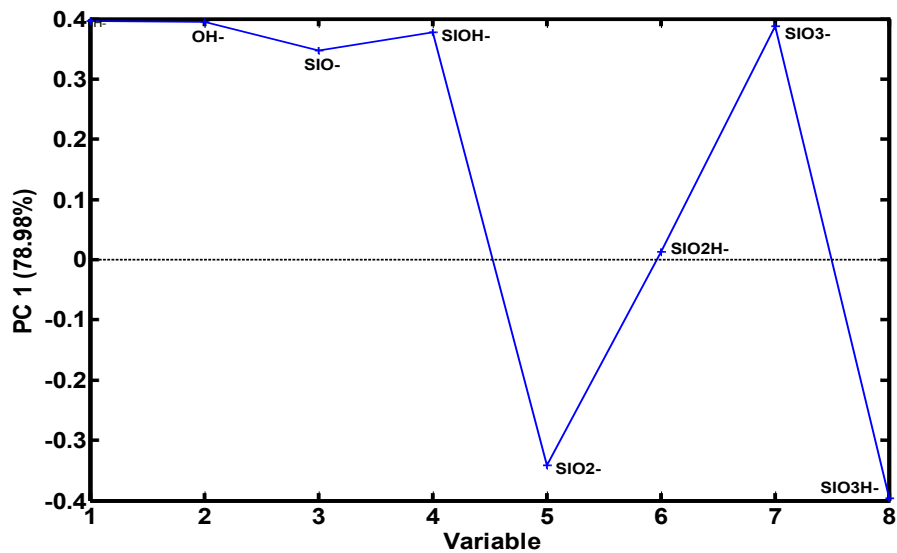
(a)
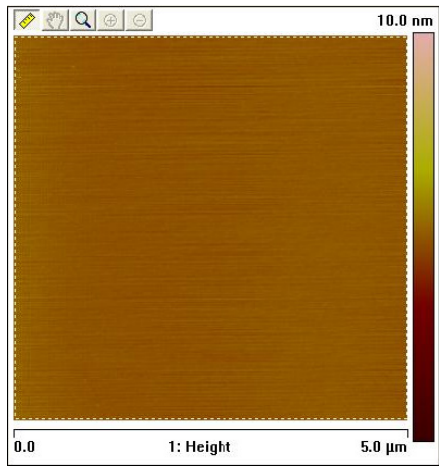
(b)
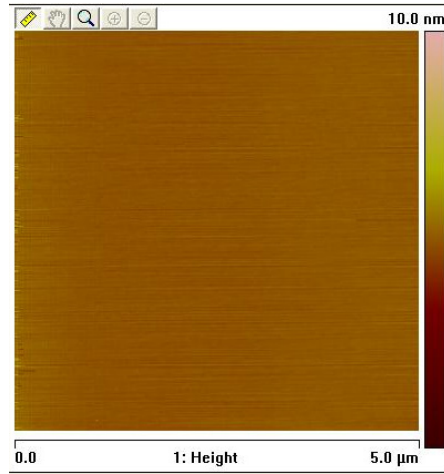
(c)
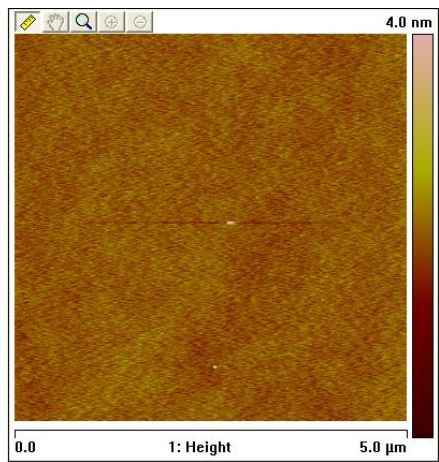
(d)

Figure I.2 AFM images (a) Before H_2 plasma treatment R_q = 1.22 Å (b) After 60 s H_2 Plasma treatment R_q = 1.27 Å. (c) Before O_2 plasma treatment R_q = 1.8 Å (d) After 60 s O_2 Plasma treatment R_q = 0.9 Å. These results indicate no change in surface roughness after hydrogen or oxygen plasma treatment.
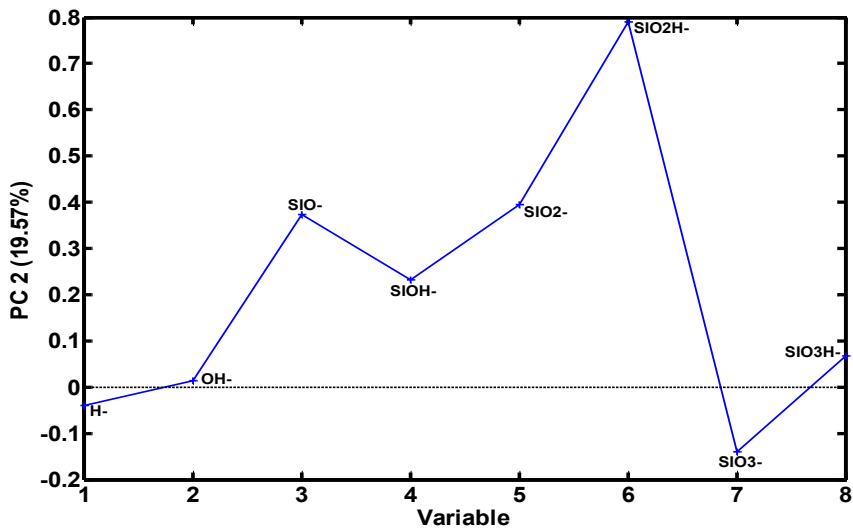
(a)

(b)

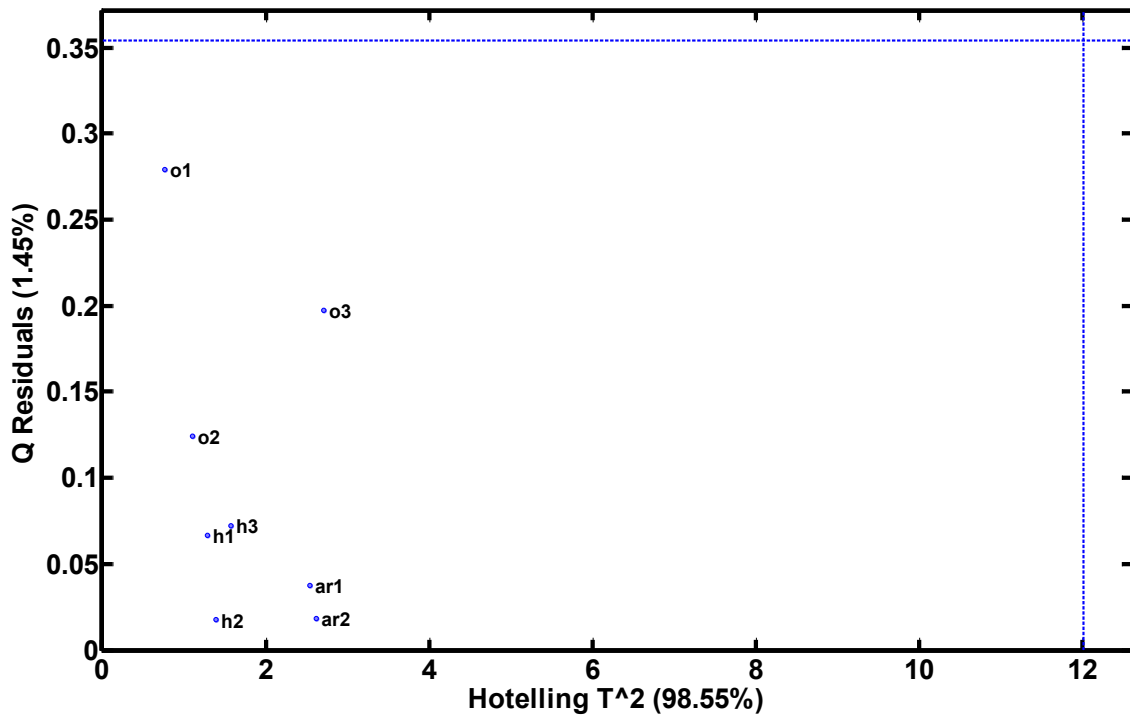Figure I.3 (a) Loadings on PC1 and (b) PC2 from PCA analysis of ToF-SIMS data.

Figure I.4 Plot of Q Residuals vs. Hotelling T^2.